

000 001 002 003 004 005 006 007 008 009 010 011 012 013 014 015 016 017 018 019 020 021 022 023 024 025 026 027 028 029 030 031 032 033 034 035 036 037 038 039 040 041 042 043 044 045 046 047 048 049 050 051 052 053 LEARNING LINEAR STATE-SPACE MODELS WITH SPARSE SYSTEM MATRICES

Anonymous authors

Paper under double-blind review

ABSTRACT

Due to tractable analysis and control, linear state-space models (LSSMs) provide a fundamental mathematical tool for time-series data modeling in various disciplines. In particular, many LSSMs have sparse system matrices because interactions among variables are limited or only a few significant relationships exist. However, current learning algorithms for LSSMs lack the ability to learn system matrices with the sparsity constraint due to the similarity transformation. To address this issue, we impose sparsity-promoting priors on system matrices to balance modeling error and model complexity. By taking hidden states of LSSMs as latent variables, we then explore the expectation–maximization (EM) algorithm to derive a maximum a posteriori (MAP) estimate of both hidden states and system matrices from noisy observations. Based on the Global Convergence Theorem, we further demonstrate that the proposed learning algorithm yields a sequence converging to a local maximum or saddle point of the joint posterior distribution. Finally, experimental results on simulation and real-world problems illustrate that the proposed algorithm can preserve the inherent topological structure among variables and significantly improve prediction accuracy over classical learning algorithms.

1 INTRODUCTION

Linear state-space models (LSSMs) are fundamental mathematical tools for analyzing time-series data with applications in robotics (Mamakoukas et al., 2019; 2020), systems biology (Jin et al., 2020b; Pillonetto & Ljung, 2023), and natural language processing (Smith et al., 1999; Belanger & Kakade, 2015). Generally, LSSMs describe time-series data $\{(\mathbf{u}_t, \mathbf{y}_t)\}_{t=1}^T$ through the following stochastic difference equation:

$$\mathbf{x}_t = \mathbf{A}\mathbf{x}_{t-1} + \mathbf{B}\mathbf{u}_t + \boldsymbol{\varepsilon}_t, \quad (1)$$

$$\mathbf{y}_t = \mathbf{C}\mathbf{x}_t + \mathbf{D}\mathbf{u}_t + \boldsymbol{\omega}_t, \quad (2)$$

where $\mathbf{u}_t \in \mathbb{R}^p$ is the input signal, $\mathbf{y}_t \in \mathbb{R}^m$ is the noisy observation, $\mathbf{x}_t \in \mathbb{R}^n$ is the hidden state, $\mathbf{A} \in \mathbb{R}^{n \times n}$, $\mathbf{B} \in \mathbb{R}^{n \times p}$, $\mathbf{C} \in \mathbb{R}^{m \times n}$, and $\mathbf{D} \in \mathbb{R}^{m \times p}$ are the unknown system matrices, and $\boldsymbol{\varepsilon}_t \sim \mathcal{N}(\mathbf{0}, \mathbf{R})$ and $\boldsymbol{\omega}_t \sim \mathcal{N}(\mathbf{0}, \mathbf{Q})$ are the diagonal process and measurement noise, respectively. In addition, LSSMs are also widely used to approximate complex non-linear systems in industrial processes given their relative simplicity (Yuan et al., 2017; Lusch et al., 2018). Due to a complete rigorous theory available on LSSMs, learning them from noisy observations can enable us to make tractable analysis and control of systems (Chen & Poor, 2022; Bakshi et al., 2023).

In this paper, we focus on learning LSSMs with sparse system matrices for two important reasons. First, the learned LSSMs should include the minimally required parameters to explain time-series data following the *Occam’s razor* principle, which favors explanations constructed with the smallest possible set of elements. Additionally, many real-world systems indeed have a sparse topology, as each state or measurement variable only depends on a few other state variables and inputs (Efroni et al., 2022). For example, a gene only regulates the expression of a limited number of other genes in gene regulatory networks (He et al., 2024b). In industry, communication systems usually have a sparse topology to reduce energy consumption (Jin et al., 2020a;b). However, available learning algorithms lack the ability to learn LSSMs with the sparsity constraint on system matrices due to the similarity transformation.

To learn LSSMs with sparse system matrices, we impose sparsity-promoting priors on them to balance model complexity and modeling error. Following the Bayes' rule, we can combine the marginal likelihood and prior functions to derive the joint posterior distribution of all the unknown variables. However, directly maximizing such a posterior distribution to estimate system matrices is intractable because the hidden states of LSSMs are unknown. To address this issue, we explore the expectation–maximization (EM) algorithm to give an alternate maximum a posteriori (MAP) estimate of hidden states and system matrices by taking hidden states as latent variables. In the expectation step, we use the Rauch–Tung–Striebel (RTS) smoother to give a closed-form update rule for the hidden states. In the maximization step, we leverage the block coordinate descent method to analytically update the system matrices in turn. By alternately performing the expectation and maximization steps until convergence, the proposed algorithm can determine the sparse system matrices of LSSMs from noisy observations. In summary, the contributions of this paper are threefold:

- Leveraging sparsity-promoting techniques, we propose an algorithm to learn LSSMs with sparse system matrices from noisy observations. Following the Global Convergence Theorem (Luenberger et al., 1984), we also demonstrate that the proposed algorithm is guaranteed to converge to a local maximum or saddle point of the posterior distribution composed of marginal likelihood and prior functions.
- Because available learning algorithms only learn LSSMs up to a similarity transformation, the learned system matrices usually differ from the true ones in both numerical values and topological structure. However, the proposed algorithm learns system matrices by balancing model complexity and modeling error. As a result, the learned system matrices can preserve the inherent topological structure among variables, which is a significant improvement over classical learning algorithms.
- Experimental results on simulation and real-world datasets demonstrate that the proposed algorithm outperforms classical ones on learning LSSMs with sparse system matrices. In addition, the learned system matrices of the proposed algorithm are more valuable for exploring the interaction laws of systems.

2 RELATED WORK

Least-squares minimization. Basically, least-squares minimization (LSM) learns unknown models by minimizing the sum of the squares of residuals (Faradonbeh et al., 2018; 2020; Modi et al., 2024). Taking one-step prediction errors as the objective function in LSM, prediction error minimization (PEM) is proposed to learn LSSMs via gradient-based optimization methods (Ljung, 2002; Katayama et al., 2005). Given a symmetric transition matrix, Hazan et al. (2017) design an efficient method for the online prediction of LSSMs by formulating system identification as an online PEM problem. Recently, combining the Ho–Klamn (HK) algorithm with LSM, Oymak & Ozay (2019) propose a method to learn system matrices of LSSMs with sample complexity analysis. However, it is well known that LSM is sensitive to noise and cannot characterize the sparsity of system matrices (Tibshirani, 1996; Martens, 2010).

Subspace state-space system identification. Subspace state-space system identification (4SID) algorithms project data Hankel matrices onto certain subspaces to estimate the extended observability matrix and hidden states using linear algebra tools (Larimore, 1990; Verahegen & Dewilde, 1992; Van Overschee & De Moor, 1994; He et al., 2024a). Subsequently, system matrices can be recovered from either the extended observability matrix or hidden states (Favoreel et al., 2000). Based on principal component analysis, Wang & Qin (2002) present a new 4SID algorithm to learn LSSMs under the errors-in-variables situation. By choosing different weighting matrices to perform the singular value decomposition, Van Overschee & De Moor (2012) provide a geometric framework to unify almost all classical 4SID methods. Further, Huang et al. (2016) present the Weight-Least-Square method to learn stable LSSMs by multiplying the unstable component with a weight matrix. However, it is widely recognized that such algorithms generally cannot obtain accurate system matrices as required (Martens, 2010; Qin, 2006).

Maximum likelihood estimation. Because the joint likelihood function of LSSMs involves hidden states, the EM algorithm is employed to give the maximum likelihood estimation (MLE) of system matrices (Shumway & Stoffer, 1982; Ghahramani & Hinton, 1996). Leveraging the EM algorithm, the distribution of hidden states can be explicitly derived using the Kalman smoother based on the

108 current estimate of system matrices. It then updates system matrices by maximizing the expected
 109 log-likelihood with respect to the hidden states. To present a robust MLE for LSSMs, Gibson &
 110 Ninness (2005) implement the expectation and maximization steps via the LR and Cholesky factori-
 111 sation, respectively. To increase the efficiency of EM for learning LSSMs, Martens (2010) proposes
 112 an approximate second-order statistics (ASOS) scheme to approximate the expectation step. Com-
 113 bining EM and Lagrangian relaxation, Umenberger et al. (2018) use semidefinite programming to
 114 optimize the tight bounds on the likelihood to learn LSSMs with model stability constraints. How-
 115 ever, such learning algorithms lack the ability to deal with sparse system matrices.

116 **Sparsity-promoting methods.** By adding a penalty term on model parameters, sparsity-promoting
 117 methods can balance model complexity and modeling error to learn systems from data (Brunton
 118 et al., 2016). Leveraging the ℓ_1 regularization term, Tibshirani (1996) proposes a method named
 119 Lasso to estimate parameters in linear models. Further, reweighted ℓ_1 minimization is proposed
 120 to enhance sparsity (Wipf & Nagarajan, 2007; Candes et al., 2008). However, solving an ℓ_1 mini-
 121 mization problem is challenging due to its non-differentiability at the origin, and these methods also
 122 require careful fine-tuning of hyperparameters. To address such issues, sparse Bayesian learning
 123 (SBL) imposes sparsity-promoting priors on model parameters to enforce sparsity (Samanta et al.,
 124 2022; Chakraborty et al., 2023). Subsequently, it maximizes the posterior distribution consisting
 125 of the likelihood function and priors to estimate model parameters and hyperparameters (Tipping,
 126 2001; Wipf & Rao, 2004). Recently, SBL has been applied to learn various systems from data,
 127 with system states being measurable yet potentially corrupted by process noise (Pan et al., 2015;
 128 Yuan et al., 2019; Wang et al., 2024). However, leveraging such sparsity-promoting methods to
 129 learn LSSMs with sparse system matrices remains an elusive and challenging problem because
 130 system states are unavailable and observed data are corrupted by both process and measurement
 131 noise (Course & Nair, 2023).

132 3 METHODOLOGY

134 Due to the similarity transformation, LSSMs admit many equivalent representations with different
 135 levels of sparsity, where the corresponding transformed system matrices are given by $\Phi \mathbf{A} \Phi^{-1}$, $\Phi \mathbf{B}$,
 136 $\mathbf{C} \Phi^{-1}$, and \mathbf{D} , with $\Phi \in \mathbb{R}^{n \times n}$ being a nonsingular matrix. However, we focus on learning the
 137 LSSMs with sparse system matrices that include minimally required parameters in accordance with
 138 the *Occam's razor* principle. Hence, we define the identifiability of LSSMs with sparse system ma-
 139 trices to ensure that the resulting ambiguities can only be permutations and scaling, as is formalized
 140 as follows.

141 **Definition 3.1. (Identifiability)** For LSSMs with nonzero system matrices $\mathbf{A}, \mathbf{B}, \mathbf{C}$, and \mathbf{D} , if any
 142 nonsingular matrix $\Phi \in \mathbb{R}^{n \times n}$ satisfying

$$143 \|\Phi \mathbf{A} \Phi^{-1}\|_0 = \|\mathbf{A}\|_0, \quad \|\Phi \mathbf{B}\|_0 = \|\mathbf{B}\|_0, \quad \text{and} \quad \|\mathbf{C} \Phi^{-1}\|_0 = \|\mathbf{C}\|_0, \quad (3)$$

144 must be a generalized permutation matrix, then such systems are said to be essentially identifiable,
 145 up to permutation and scaling.

147 3.1 STUDENT'S t -DISTRIBUTION PRIOR

149 Here, we impose the Student's t -distribution prior on the system matrices $\mathbf{A}, \mathbf{B}, \mathbf{C}$, and \mathbf{D} to pro-
 150 mote model sparsity, because it can be sharply peaked at zero compared to other priors (Tipping,
 151 2001). Generally, the Student's t -distribution prior is implemented in a hierarchical way (Wang
 152 et al., 2024; Zhou et al., 2021). It imposes a zero-mean Gaussian prior on the system matrices and
 153 then adopts an Inverse-Gamma distribution on the unknown variance. For example, we can impose
 154 the Student's t -distribution prior on \mathbf{A} to promote its sparsity as follows:

$$155 p(\mathbf{A} \mid \Gamma_a) = \prod_{i=1}^n \prod_{j=1}^n p(A_{ij} \mid \Gamma_{a,ij}) = \prod_{i=1}^n \prod_{j=1}^n \frac{1}{\sqrt{2\pi\Gamma_{a,ij}}} \exp\left(-\frac{A_{ij}^2}{2\Gamma_{a,ij}}\right), \quad (4)$$

$$158 p(\Gamma_a) = \prod_{i=1}^n \prod_{j=1}^n \frac{a_0^{b_0}}{\Gamma(a_0)} \Gamma_{a,ij}^{-a_0-1} \exp\left(-\frac{b_0}{\Gamma_{a,ij}}\right), \quad (5)$$

161 where $\Gamma(\cdot)$ is the gamma function, and A_{ij} and $\Gamma_{a,ij}$ are the ij th components of \mathbf{A} and Γ_a , respec-
 162 tively. To generate non-informative hyperprior on $\Gamma_{a,ij}$, a_0 and b_0 are typically set to very small

162 values (e.g., 10^{-6}). In addition, Γ_b , Γ_c , Γ_d , $\Gamma_{b,ij}$, $\Gamma_{c,ij}$, and $\Gamma_{d,ij}$ are defined in a similar manner (see Appendix A). For the process noise \mathbf{R} and measurement noise \mathbf{Q} , we impose a uniform distribution prior on them to derive a flat prior.
163
164
165

166 3.2 LOSS FUNCTION 167

168 Following the Bayes' rule, we can combine the marginal likelihood and prior functions to derive the
169 joint posterior distribution of all the unknown variables as follows:
170
171

$$p(\Theta | \mathbf{Y}) \propto \underbrace{p(\mathbf{Y} | \Theta)}_{\text{marginal likelihood}} \times \underbrace{p(\Theta)}_{\text{prior}}, \quad (6)$$

172 where $\Theta = \{\mathbf{A}, \mathbf{B}, \mathbf{C}, \mathbf{D}, \mathbf{R}, \mathbf{Q}, \Gamma_a, \Gamma_b, \Gamma_c, \Gamma_d\}$ is the set of unknown variables and $\mathbf{Y} = [y_1, y_2, \dots, y_T]$. Because the system state \mathbf{x}_t is unobserved, it is hard to explicitly compute $p(\mathbf{Y} | \Theta)$. Hence, directly maximizing equation 6 to estimate Θ is generally intractable. To tackle this problem, we explore the EM algorithm to iteratively improve equation 6 by regarding \mathbf{x}_t as the latent variable. Instead of directly maximizing equation 6, the EM algorithm focuses on improving the expected value of the log posterior function of Θ with respect to the state vector $\mathbf{X} = [\mathbf{x}_1, \mathbf{x}_2, \dots, \mathbf{x}_T]$ as follows:
173
174
175
176
177
178
179

$$H(\Theta | \Theta^k) = \mathbb{E}_{\mathbf{X}^k} [\log(p(\mathbf{Y}, \mathbf{X} | \Theta)p(\Theta))], \quad (7)$$

180 where $\mathbf{X}^k \sim p(\mathbf{X} | \mathbf{Y}, \Theta^k)$, and \mathbf{X}^k and Θ^k denote the estimates of \mathbf{X} and Θ at the k th iteration, respectively. It is well-known that iteratively maximizing equation 7 is equivalent to iteratively maximizing equation 6 (Little & Rubin, 2019).
181
182
183
184
185

186 3.3 EXPECTATION STEP: RAUCH–TUNG–STRIEBEL SMOOTHING 187

188 Because equation 7 involves $p(\mathbf{X} | \mathbf{Y}, \Theta^k)$, we first need to derive the conditional distribution of \mathbf{x}_t given \mathbf{Y} and current $\Theta^k = \{\mathbf{A}^k, \mathbf{B}^k, \mathbf{C}^k, \mathbf{D}^k, \mathbf{R}^k, \mathbf{Q}^k, \Gamma_a^k, \Gamma_b^k, \Gamma_c^k, \Gamma_d^k\}$, which can be formulated as a classical smoothing problem. For LSSMs, the RTS smoother provides a closed-form smoothing solution for $p(\mathbf{x}_t | \mathbf{Y}, \Theta^k)$.
189
190
191
192

Lemma 3.1. (RTS smoother Särkkä & Svensson (2023)) For LSSMs, the RTS smoother states that

$$p(\mathbf{x}_t | \mathbf{Y}, \Theta^k) = \mathcal{N}(\mathbf{m}_t^k, \mathbf{P}_t^k), \quad (8)$$

193 where $t = 0, \dots, T$. Here, \mathbf{m}_t^k and \mathbf{P}_t^k are derived via the reverse-time recursions as follows:
194
195

$$\mathbf{m}_t^k = \boldsymbol{\mu}_t^k + \mathbf{G}_t^k (\mathbf{m}_{t+1}^k - \bar{\boldsymbol{\mu}}_{t+1}^k), \quad (9)$$

$$\mathbf{P}_t^k = \boldsymbol{\Sigma}_t^k + \mathbf{G}_t^k (\mathbf{P}_{t+1}^k - \bar{\boldsymbol{\Sigma}}_{t+1}^k) (\mathbf{G}_t^k)', \quad (10)$$

200 where $\mathbf{G}_t^k = \boldsymbol{\Sigma}_t^k (\mathbf{A}^k)' (\bar{\boldsymbol{\Sigma}}_{t+1}^k)^{-1}$. The quantities $\boldsymbol{\mu}_t^k$, $\bar{\boldsymbol{\mu}}_t^k$, $\boldsymbol{\Sigma}_t^k$, and $\bar{\boldsymbol{\Sigma}}_t^k$ coupled in equation 9 and equation 10 are pre-computed using the Kalman filter as follows:
201
202
203

$$\bar{\boldsymbol{\mu}}_t^k = \mathbf{A}^k \boldsymbol{\mu}_{t-1}^k + \mathbf{B}^k \mathbf{u}_t, \quad \bar{\boldsymbol{\Sigma}}_t^k = \mathbf{A}^k \boldsymbol{\Sigma}_{t-1}^k (\mathbf{A}^k)' + \mathbf{R}^k, \quad (11)$$

$$\mathbf{K}_t^k = \bar{\boldsymbol{\Sigma}}_t^k (\mathbf{C}^k)' (\mathbf{C}^k \bar{\boldsymbol{\Sigma}}_t^k (\mathbf{C}^k)' + \mathbf{Q}^k)^{-1}, \quad (12)$$

$$\boldsymbol{\mu}_t^k = \bar{\boldsymbol{\mu}}_t^k + \mathbf{K}_t^k (\mathbf{Y}_t - \mathbf{C}^k \bar{\boldsymbol{\mu}}_t^k - \mathbf{D}^k \mathbf{u}_t), \quad \boldsymbol{\Sigma}_t^k = (\mathbf{I}_n - \mathbf{K}_t^k \mathbf{C}^k) \bar{\boldsymbol{\Sigma}}_t^k, \quad (13)$$

204 where \mathbf{I}_n is an identity matrix of dimension n . Note that the reverse-time recursions of equation 9 and equation 10 start from the initial conditions $\mathbf{m}_T^k = \boldsymbol{\mu}_T^k$ and $\mathbf{P}_T^k = \boldsymbol{\Sigma}_T^k$, and the recursions of equation 11–equation 13 start from the mean $\boldsymbol{\mu}_0^k$ and covariance $\boldsymbol{\Sigma}_0^k$ of the initial state \mathbf{x}_0 .
205
206
207

208 Besides $p(\mathbf{x}_t | \mathbf{Y}, \Theta^k)$, we also need to derive the covariance matrix between the adjacent states \mathbf{x}_t and \mathbf{x}_{t-1} given \mathbf{Y} and Θ^k to compute equation 7. To address this issue, the following lemma gives necessary recursions.
209
210
211
212
213

216 **Lemma 3.2.** (The lag-one covariance smoother Särkkä & Svensson (2023)) For LSSMs, the covariance
 217 matrix $\mathbf{P}_{t,t-1}^k$ between the adjacent states \mathbf{x}_t and \mathbf{x}_{t-1} given \mathbf{Y} and Θ^k can be recursively
 218 derived as follows:

$$219 \quad 220 \quad \mathbf{P}_{t,t-1}^k = (\Sigma_t^k + \mathbf{G}_t^k \mathbf{P}_{t+1,t}^k - \mathbf{G}_t^k \mathbf{A}^k \Sigma_t^k) (\mathbf{G}_{t-1}^k)' \quad (14)$$

221 with $\mathbf{P}_{T,T-1}^k = (\mathbf{I}_n - \mathbf{K}_T^k \mathbf{C}^k) \mathbf{A}^k \Sigma_{T-1}^k$.

222 Based on Lemmas 3.1 and 3.2, we are able to calculate the loss function in equation 7 as follows:

$$224 \quad H(\Theta | \Theta^k) = H_1(\mathbf{A}, \mathbf{B}, \mathbf{R}) + H_2(\mathbf{C}, \mathbf{D}, \mathbf{Q}) + H_3(\mathbf{A}, \mathbf{B}, \mathbf{C}, \mathbf{D}, \Gamma_a, \Gamma_b, \Gamma_c, \Gamma_d), \quad (15)$$

225 where

$$226 \quad 227 \quad H_1(\mathbf{A}, \mathbf{B}, \mathbf{R}) = \mathbb{E}_{\mathbf{X}^k} [\log p(\mathbf{X} | \mathbf{A}, \mathbf{B}, \mathbf{R})], \quad (16)$$

$$228 \quad H_2(\mathbf{C}, \mathbf{D}, \mathbf{Q}) = \mathbb{E}_{\mathbf{X}^k} [\log p(\mathbf{Y} | \mathbf{X}, \mathbf{C}, \mathbf{D}, \mathbf{Q})], \quad (17)$$

$$229 \quad H_3(\mathbf{A}, \mathbf{B}, \mathbf{C}, \mathbf{D}, \Gamma_a, \Gamma_b, \Gamma_c, \Gamma_d) = \mathbb{E}_{\mathbf{X}^k} [\log (p(\mathbf{A}, \Gamma_a) p(\mathbf{B}, \Gamma_b) p(\mathbf{C}, \Gamma_c) p(\mathbf{D}, \Gamma_d))]. \quad (18)$$

230 Due to the limited space, the detailed derivation of equation 15 and explicit mathematical expressions
 231 of $H_1(\mathbf{A}, \mathbf{B}, \mathbf{R})$, $H_2(\mathbf{C}, \mathbf{D}, \mathbf{Q})$, and $H_3(\mathbf{A}, \mathbf{B}, \mathbf{C}, \mathbf{D}, \Gamma_a, \Gamma_b, \Gamma_c, \Gamma_d)$ are given in Appendix
 232 B.1.

233 3.4 MAXIMIZATION STEP: BLOCK COORDINATE DESCENT

235 Obviously, $H(\Theta | \Theta^k)$ is a non-convex function and unknown variables are highly coupled. To
 236 provide analytical update formulas, we leverage the block coordinate descent method to sequentially
 237 optimize the model parameters.

238 **Update procedures of \mathbf{A} , \mathbf{B} , \mathbf{C} , and \mathbf{D} .** Due to the introduction of sparsity-promoting priors,
 239 it is intractable to derive closed-form solutions for \mathbf{A} , \mathbf{B} , \mathbf{C} , and \mathbf{D} by setting the derivatives of
 240 $H(\Theta | \Theta^k)$ with respect to these variables to zero directly. To address this issue, we adopt a row-
 241 wise update rule for \mathbf{A} , \mathbf{B} , \mathbf{C} , and \mathbf{D} . For example, the derivative of $H(\Theta | \Theta^k)$ with respect to
 242 the r th row of \mathbf{A} , denoted as \mathbf{A}_r , is as follows:

$$244 \quad \frac{\partial (H_1(\mathbf{A}, \mathbf{B}^k, \mathbf{R}^k) + H_3(\mathbf{A}, \mathbf{B}^k, \mathbf{C}^k, \mathbf{D}^k, \Gamma_a^k, \Gamma_b^k, \Gamma_c^k, \Gamma_d^k))}{\partial \mathbf{A}_r} \\ 245 \quad = \sum_{t=1}^T (\mathbf{R}_{rr}^k)^{-1} \left((\mathbf{m}_{t,r}^k - \mathbf{A}_r \mathbf{m}_{t-1}^k - \mathbf{B}_r^k \mathbf{u}_t) (\mathbf{m}_{t-1}^k)' + (\mathbf{P}_{t,t-1,r}^k - \mathbf{A}_r \mathbf{P}_{t-1}^k) \right) - \mathbf{A}_r \bar{\Gamma}_{a,r}^{kd}, \quad (19)$$

250 where \mathbf{R}_{rr}^k is the rr th component of \mathbf{R}^k , $\mathbf{P}_{t,t-1,r}^k$, $\mathbf{m}_{t,r}^k$, and \mathbf{B}_r^k are the r th rows of $\mathbf{P}_{t,t-1}^k$, \mathbf{m}_t^k ,
 251 and \mathbf{B}^k , respectively. In particular, $\bar{\Gamma}_{a,r}^{kd} = \text{diag}[\bar{\Gamma}_{a,r}^k]$ with $\bar{\Gamma}_{a,r}^k$ being the r th row of $\bar{\Gamma}_a^k$. Setting
 252 equation 19 to zero leads to the following update rule for \mathbf{A}_r at the k th iteration:

$$254 \quad 255 \quad \mathbf{A}_r^{k+1} = \left(\sum_{t=1}^T \left((\mathbf{m}_{t,r}^k - \mathbf{B}_r^k \mathbf{u}_t) (\mathbf{m}_{t-1}^k)' + \mathbf{P}_{t,t-1,r}^k \right) \right)^{-1} \\ 256 \quad 257 \quad \times \left(\sum_{t=1}^T \left(\mathbf{P}_{t-1}^k + \mathbf{m}_{t-1}^k (\mathbf{m}_{t-1}^k)' \right) + \mathbf{R}_{rr}^k \bar{\Gamma}_{a,r}^{kd} \right)^{-1}. \quad (20)$$

258 The detailed derivation of equation 19 can be found in Appendix B.2. Similarly, we can update the
 259 r th row of \mathbf{B} , \mathbf{C} , and \mathbf{D} at the k th iteration as follows:

$$262 \quad \mathbf{B}_r^{k+1} = \left(\sum_{t=1}^T (\mathbf{m}_{t,r}^k - \mathbf{A}_r^{k+1} \mathbf{m}_{t-1}^k) \mathbf{u}_t' \right) \left(\sum_{t=1}^T \mathbf{u}_t \mathbf{u}_t' + \mathbf{R}_{rr}^k \bar{\Gamma}_{b,r}^{kd} \right)^{-1}, \quad (21)$$

$$265 \quad \mathbf{C}_r^{k+1} = \left(\sum_{t=1}^T (\mathbf{y}_{t,r} - \mathbf{D}_r^k \mathbf{u}_t) (\mathbf{m}_t^k)' \right) \left(\sum_{t=1}^T (\mathbf{P}_t^k + \mathbf{m}_t^k (\mathbf{m}_t^k)') + \mathbf{Q}_{rr}^k \bar{\Gamma}_{c,r}^{kd} \right)^{-1}, \quad (22)$$

$$268 \quad \mathbf{D}_r^{k+1} = \left(\sum_{t=1}^T (\mathbf{y}_{t,r} - \mathbf{C}_r^{k+1} \mathbf{m}_t^k) \mathbf{u}_t' \right) \left(\sum_{t=1}^T \mathbf{u}_t \mathbf{u}_t' + \mathbf{Q}_{rr}^k \bar{\Gamma}_{d,r}^{kd} \right)^{-1}, \quad (23)$$

270 where $\mathbf{y}_{t,r}$ is the r th component of \mathbf{y}_t , \mathbf{Q}_{rr}^k is the rr th component of \mathbf{Q}^k , and $\bar{\mathbf{\Gamma}}_{b,r}^{kd}$, $\bar{\mathbf{\Gamma}}_{c,r}^{kd}$, and $\bar{\mathbf{\Gamma}}_{d,r}^{kd}$ are defined as that of $\bar{\mathbf{\Gamma}}_{a,r}^{kd}$.

273 **Update procedures of \mathbf{R} and \mathbf{Q} .** The derivative of $H(\Theta | \Theta^k)$ with respect to the rr th component of \mathbf{R} , denoted as \mathbf{R}_{rr} , is as follows (see Appendix B.3):

$$276 \frac{\partial H_1(\mathbf{A}^{k+1}, \mathbf{B}^{k+1}, \mathbf{R})}{\partial \mathbf{R}_{rr}} = -\frac{T}{2\mathbf{R}_{rr}} + \frac{\sum_{t=1}^T (\pi_{t,r}^k)^2 + \sum_{t=1}^T \Pi_{t,rr}^k}{2\mathbf{R}_{rr}^2}, \quad (24)$$

279 where

$$280 \pi_t^k = \mathbf{m}_t^k - \mathbf{A}^{k+1} \mathbf{m}_{t-1}^k - \mathbf{B}^{k+1} \mathbf{u}_t, \quad (25)$$

$$281 \Pi_t^k = \mathbf{P}_t^k - \mathbf{A}^{k+1} \mathbf{P}_{t-1}^k - \mathbf{P}_{t-1}^k (\mathbf{A}^{k+1})' + \mathbf{A}^{k+1} \mathbf{P}_{t-1}^k (\mathbf{A}^{k+1})' \quad (26)$$

283 with $\pi_{t,r}^k$ and $\Pi_{t,rr}^k$ being the r th and rr th components of π_t^k and Π_t^k , respectively. Setting equation 24 to zero yields the following update rule for \mathbf{R}_{rr} at the k th iteration:

$$286 \mathbf{R}_{rr}^{k+1} = \frac{\sum_{t=1}^T (\pi_{t,r}^k)^2 + \sum_{t=1}^T \Pi_{t,rr}^k}{T}. \quad (27)$$

288 Similarly, we can update the rr th component of \mathbf{Q} , denoted as \mathbf{Q}_{rr} , at the k th iteration as follows:

$$290 \mathbf{Q}_{rr}^{k+1} = \frac{\sum_{t=1}^T (\psi_{t,r}^k)^2 + \sum_{t=1}^T \Psi_{t,rr}^k}{T}, \quad (28)$$

292 where

$$294 \psi_t^k = \mathbf{y}_t - \mathbf{C}^{k+1} \mathbf{m}_t^k - \mathbf{D}^{k+1} \mathbf{u}_t, \quad \Psi_t^k = \mathbf{C}^{k+1} \mathbf{P}_t^k (\mathbf{C}^{k+1})' \quad (29)$$

295 with $\psi_{t,r}^k$ and $\Psi_{t,rr}^k$ being the r th and rr th components of ψ_t^k and Ψ_t^k , respectively.

297 **Update procedures of $\mathbf{\Gamma}_a$, $\mathbf{\Gamma}_b$, $\mathbf{\Gamma}_c$, and $\mathbf{\Gamma}_d$.** Because each component of $\mathbf{\Gamma}_a$, $\mathbf{\Gamma}_b$, $\mathbf{\Gamma}_c$, and $\mathbf{\Gamma}_d$ is 298 independent of the others, we can update them individually. For example, we can calculate the 299 derivative of $H(\Theta | \Theta^k)$ with respect to $\mathbf{\Gamma}_{a,ij}$ at the k th iteration as follows:

$$300 \frac{\partial H_3(\mathbf{A}^{k+1}, \mathbf{B}^{k+1}, \mathbf{C}^{k+1}, \mathbf{D}^{k+1}, \mathbf{\Gamma}_a, \mathbf{\Gamma}_b^k, \mathbf{\Gamma}_c^k, \mathbf{\Gamma}_d^k)}{\partial \mathbf{\Gamma}_{a,ij}} = -\frac{2a_0 + 3}{2\mathbf{\Gamma}_{a,ij}} + \frac{(\mathbf{A}_{ij}^{k+1})^2 + 2b_0}{2\mathbf{\Gamma}_{a,ij}^2}. \quad (30)$$

303 Setting equation 30 to zero and solving for $\mathbf{\Gamma}_{a,ij}$ leads to:

$$305 \mathbf{\Gamma}_{a,ij}^{k+1} = \frac{(\mathbf{A}_{ij}^{k+1})^2 + 2b_0}{2a_0 + 3}. \quad (31)$$

308 Similarly, we can update each component of $\mathbf{\Gamma}_b$, $\mathbf{\Gamma}_c$, and $\mathbf{\Gamma}_d$ at the k th iteration as follows:

$$309 \mathbf{\Gamma}_{b,ij}^{k+1} = \frac{(\mathbf{B}_{ij}^{k+1})^2 + 2b_0}{2a_0 + 3}, \quad \mathbf{\Gamma}_{c,ij}^{k+1} = \frac{(\mathbf{C}_{ij}^{k+1})^2 + 2b_0}{2a_0 + 3}, \quad \mathbf{\Gamma}_{d,ij}^{k+1} = \frac{(\mathbf{D}_{ij}^{k+1})^2 + 2b_0}{2a_0 + 3}. \quad (32)$$

312 Finally, we summarize the procedure for learning LSSMs with sparse system matrices in Appendix 313 C.

315 3.5 GLOBAL CONVERGENCE ANALYSIS

316 Given Θ^k , the proposed learning algorithm presents the analytical mathematical expressions to 317 derive Θ^{k+1} . Hence, we can define the proposed algorithm as a point-to-point mapping $\mathcal{A}(\cdot)$. Lever- 318 aging the Global Convergence Theorem (Luenberger et al., 1984), we can demonstrate that the 319 proposed algorithm is globally convergent.

321 **Theorem 3.3.** *From any valid initialization point Θ^0 , the limit point of the sequence $\{\Theta^k\}_{k=1}^\infty$ 322 generated via $\Theta^{k+1} = \mathcal{A}(\Theta^k)$ is a local maximum (or saddle point) of equation 6.*

323 *Proof.* See Appendix D. □

324 4 SIMILARITY TRANSFORMATION OF LSSMs

326 The similarity transformation provides an equivalent realization of original LSSMs by transforming
 327 states into different coordinate systems. For LSSMs, it is an important mathematical operation
 328 to analyze system properties like controllability, observability, and stability. Specifically, we can
 329 transform the state vector \mathbf{x}_t into a new state vector $\bar{\mathbf{x}}_t$ through the relation $\bar{\mathbf{x}}_t = \Phi \mathbf{x}_t$, where
 330 $\Phi \in \mathbb{R}^{n \times n}$ is a nonsingular matrix. As such, we can derive an equivalent realization of the original
 331 LSSMs as follows (see Appendix E):

$$332 \quad \bar{\mathbf{x}}_t = \bar{\mathbf{A}} \bar{\mathbf{x}}_{t-1} + \bar{\mathbf{B}} \mathbf{u}_t + \bar{\varepsilon}_t, \quad (33)$$

$$334 \quad \mathbf{y}_t = \bar{\mathbf{C}} \bar{\mathbf{x}}_t + \mathbf{D} \mathbf{u}_t + \boldsymbol{\omega}_t, \quad (34)$$

335 where

$$337 \quad \bar{\mathbf{A}} = \Phi \mathbf{A} \Phi^{-1}, \quad \bar{\mathbf{B}} = \Phi \mathbf{B}, \quad \bar{\mathbf{C}} = \mathbf{C} \Phi^{-1}, \quad (35)$$

338 and $\bar{\varepsilon}_t \sim \mathcal{N}(\mathbf{0}, \Phi \mathbf{R} \Phi')$. However, the similarity transformation makes it particularly difficult to
 339 accurately learn system matrices. Given the input signals $\{\mathbf{u}_t\}_{t=1}^T$, the transformed LSSMs can pro-
 340 duce the same output data $\{\mathbf{y}_t\}_{t=1}^T$ as the original LSSMs. Hence, classical learning algorithms for
 341 LSSMs only learn the system matrices up to a similar transformation (Viberg, 1994). For LSSMs
 342 with sparse system matrices, such a transformation changes not only the numerical values but, more
 343 importantly, the topological structure of the system matrices, resulting in misinterpretation of in-
 344 trinsic working mechanisms.

345 4.1 BENEFIT OF SPARSITY-PROMOTING PRIORS

346 Unlike classical learning algorithms, the proposed algorithm learns LSSMs with sparse system ma-
 347 trices by adopting a sparsity-promoting prior to balance model complexity and modeling error.
 348 Given the sparsity constraint of system matrices, the similarity transformation cannot be applied
 349 using any arbitrary nonsingular matrix Φ . For the identifiable LSSMs, the nonsingular matrix is
 350 restricted to be a generalized permutation matrix; otherwise, the transformed LSSMs will include
 351 redundant parameters to describe the systems. For example, consider the LSSMs with sparse system
 352 matrices as follows:

$$354 \quad \mathbf{A} = \begin{bmatrix} 0 & 0 & 0.8 \\ 0.8 & 0 & 0 \\ 0 & 0.8 & 0 \end{bmatrix}, \quad \mathbf{B} = \begin{bmatrix} 2 & 0 & 0 \\ 0 & 2 & 0 \\ 0 & 0 & 2 \end{bmatrix}, \quad \mathbf{C} = \begin{bmatrix} 2 & 0 & 0 \\ 0 & 0 & 2 \\ 0 & 2 & 0 \end{bmatrix}, \quad \mathbf{D} = \begin{bmatrix} 0 & 2 & 0 \\ 0 & 0 & 2 \\ 2 & 0 & 0 \end{bmatrix}. \quad (36)$$

355 It is easy to verify that such a system is identifiable, as the rank of system matrices is equal to the
 356 number of nonzero components. Hence, we can derive that the nonsingular matrix Φ must be one
 357 of the following generalized permutation matrices:

$$361 \quad \begin{bmatrix} a & 0 & 0 \\ 0 & b & 0 \\ 0 & 0 & c \end{bmatrix}, \quad \begin{bmatrix} a & 0 & 0 \\ 0 & 0 & b \\ 0 & c & 0 \end{bmatrix}, \quad \begin{bmatrix} 0 & a & 0 \\ b & 0 & 0 \\ 0 & 0 & c \end{bmatrix}, \quad \begin{bmatrix} 0 & a & 0 \\ 0 & 0 & b \\ c & 0 & 0 \end{bmatrix}, \quad \begin{bmatrix} 0 & 0 & a \\ b & 0 & 0 \\ 0 & c & 0 \end{bmatrix}, \quad \begin{bmatrix} 0 & 0 & a \\ 0 & b & 0 \\ c & 0 & 0 \end{bmatrix}, \quad (37)$$

362 where a , b , and c are arbitrary constants. As such, the transformed system matrices $\bar{\mathbf{A}}$, $\bar{\mathbf{B}}$, and $\bar{\mathbf{C}}$ do
 363 not introduce additional parameters to increase model complexity.

364 Note that applying the similarity transformation with a generalized permutation matrix to the original
 365 state variables will scale their magnitudes and reorder them. However, it will scale the nonzero
 366 components and permute the rows or columns of system matrices accordingly. Hence, an additional
 367 advantage of the sparsity-promoting prior is its ability to preserve the inherent topological structure
 368 among the variables. While the learned system matrices differ from the true ones in numerical
 369 values, such a difference is only caused by the scaled definition of state variables, rather than a
 370 failure to capture the underlying system dynamics.

374 5 EXPERIMENT

375 In this section, we validate the proposed algorithm on simulation and real-world datasets. In addi-
 376 tion, we compare the proposed algorithm with classical ones mentioned previously to demonstrate

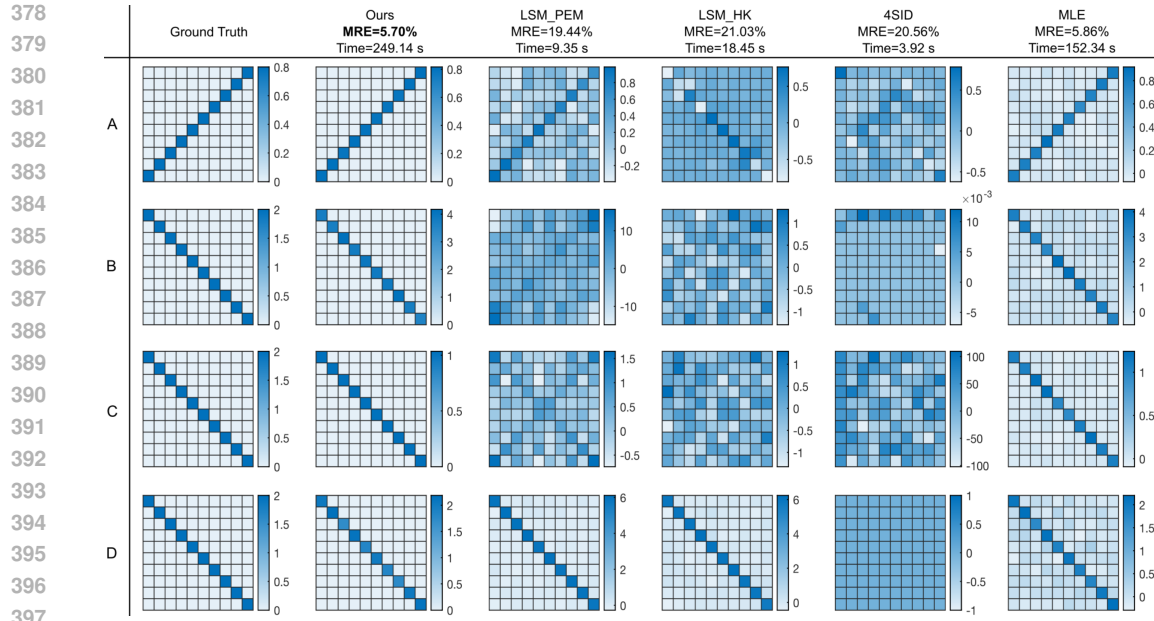


Figure 1: Experimental results of all the algorithms on the 10-dimensional synthetic system. Compared to the ground truth, only the proposed algorithm preserves the topological structure among the variables with $\Phi \approx 2\mathbf{I}_{10}$. In addition, the proposed algorithm obtains the lowest MRE among all the algorithms. Experimental results on the more complex **non-diagonal** and **non-invertible** cases can be found in Appendix I.1 and Appendix I.2, respectively.

its superior performance, including LSM_PEM, LSM_HK, 4SID, and MLE. In all experiments, the dataset is split into training and testing sets with a 2:1 ratio, where 66.7% of the data is used for training and 33.3% for testing. Due to the lack of ground truth for real-world datasets, we use the mean relative error (MRE) to evaluate the performance of all the algorithms defined as follows:

$$\text{MRE} = \sum_{t=1}^T \frac{\|\mathbf{y}_t - \hat{\mathbf{y}}_t\|_2^2}{T\|\mathbf{y}_t\|_2^2}$$
, where $\{\hat{\mathbf{y}}_t\}_{t=1}^T$ is the sequence of data points generated by the learned LSSMs in response to the same input signals. The experiments are conducted using MATLAB 2022b on the PC with an Apple M1 Pro chip with 10-core CPU and 32GB RAM. Experimental results on simulation and real-world problems illustrate that the proposed algorithm can preserve the inherent topological structure among variables and significantly improve prediction accuracy over the classical ones. **However, because the closed-form updates entail the inversion of a large number of matrices, the proposed algorithm involves high computational complexity (see Appendix F).**

5.1 SYNTHETIC SYSTEMS

First, we test all the algorithms on a 10-dimensional synthetic system, indicating that each system matrix has 100 unknown parameters. Specifically, we consider \mathbf{A} to be an anti-diagonal matrix with nonzero components equal to 0.8, and set $\mathbf{B} = \mathbf{C} = \mathbf{D} = 2\mathbf{I}_{10}$ and $\mathbf{R} = \mathbf{Q} = 0.81\mathbf{I}_{10}$. Because these system matrices are extremely sparse, accurately learning their topological structures is particularly challenging. To generate data points, the value of \mathbf{x}_0 is drawn from the Gaussian distribution with the mean $\text{diag}[\mathbf{I}_{10}]$ and an identity covariance matrix, and the input signal \mathbf{u}_t is drawn from the uniform distribution on $[0, 2]$. As for algorithm implementation, we collect 2,100 data points and set the initial value of \mathbf{A} , \mathbf{B} , \mathbf{C} , \mathbf{D} , \mathbf{R} , and \mathbf{Q} both to be \mathbf{I}_{10} . Because the iterative numerical optimization method rarely yields exact zeros, the learned parameters below the predefined threshold are truncated to zero to accelerate convergence. **The threshold selection procedure can be found in Appendix G. To ensure a fair comparison, the learned parameters of all the other algorithms that fall below this threshold are likewise set to zero.**

Because the system matrices of the synthetic system are known, we can compare the learned system matrices with real ones directly. **Figure 1 shows the learned system matrices of all the algorithms,**

432

433

Table 1: Comparison results on the real-world industrial process systems

434

435

Dataset	Ours	LSM_PEM	LSM_HK	4SID	MLE
Evaporation system	14.93% (249.14 s)	17.90% (9.35 s)	Inf (18.45 s)	43.77% (3.92 s)	20.14% (152.34 s)
Glass furnace	23.63% (45.62 s)	62.62% (0.52 s)	31.21% (6.20 s)	24.32% (0.29 s)	30.21% (33.36 s)
Steam generator	20.70% (441.88 s)	22.70% (4.94 s)	39.80% (84.52 s)	29.26% (0.58 s)	22.23% (299.10 s)

436

437

together with the associated MRE and running time. Obviously, the learned system matrices of classical algorithms are completely different with the original ones in both numerical values and topological structures due to the similarity transformation, making it difficult for us to understand the system. However, sparsity-promoting priors will restrict the nonsingular matrix Φ of the similarity transformation to be a generalized permutation matrix for this system. By comparing the learned \bar{B} and C of the proposed algorithm with real ones, we can derive $\Phi \approx 2I_{10}$, which is indeed consistent with the analysis in Section 4.1. Hence, the learned system matrices of the proposed algorithm preserve the inherent topological structure among the variables, differing only in numerical values due to the scaled definition of state variables.

438

439

We test the proposed algorithm on different initial values to demonstrate its robustness in Appendix H.1. We also conduct 20 independent trials to report the success rates of all the algorithms in learning the topological structure of the system matrices and the average MRE in Appendix H.2; experimental results illustrate that the proposed algorithm is stable across multiple runs.

440

441

In addition, we further demonstrate the effectiveness of the proposed algorithm on the **non-diagonal** and **non-invertible** cases in Appendix I.1 and Appendix I.2, respectively.

442

443

5.2 INDUSTRIAL PROCESS SYSTEMS

444

445

Next, we validate the proposed algorithm on the real-world datasets obtained from the Database for the Identification of Systems, which are standard datasets used for learning LSSMs (Zhu et al., 1994; Martens, 2010). While underlying physical systems may be non-linear, the learned LSSMs can provide a linear approximation of systems, enabling tractable analysis and control. To empirically ensure the performance of all the algorithms, we prefer to select datasets that contain at least 1,000 sample points and have multi-dimensional inputs and outputs.

446

448

Evaporation System. In industry, multiple-stage evaporators are widely used to reduce the water content of a product such as milk. The dataset is composed of 3-dimensional time-series with a length of 6,305. The inputs consist of the feed flow, vapor flow to the first evaporator stage, and cooling water flow to the condenser, while the outputs include the dry matter content, flow rate, and temperature of the product.

449

450

Glass Furnace. The second dataset comes from the Philips glass furnace, which is used to melt raw materials into glass. The glass furnace has two burners and one ventilator. Hence, the dataset includes two heating inputs and one cooling input with a length of 1,247. In addition, we collect three outputs from temperature sensors in a cross section of the furnace.

451

452

Steam Generator. The dataset comes from a boiler at Abbott Power Plant in Champaign IL, which is a dual-fuel (oil and gas) combustion unit used for both heating and electricity generation. It consists of four inputs (i.e., air flow rate, fuel flow rate, feedwater flow rate, and disturbance) and four outputs (i.e., drum pressure, excess oxygen, drum water level, and steam flow) with a length of 9,600.

453

454

Table 1 displays the MRE between the predicted outputs of all the learned LSSMs and the real one, and records the running time of each algorithm. Due to the lack of ground truth, the learned system matrices of all the algorithms are not depicted for comparison. Because the proposed algorithm obtains minimum MRE across all the datasets, experimental results demonstrate its superiority over the classical ones in real-world applications. Note that the hidden states can be defined in different

486 coordinate systems as discussed in Section 4. As a result, the learned system matrices of classical
 487 algorithms may differ from the ground truth in both numerical values and topological structures.
 488 However, the proposed algorithm learns the system matrices by balancing model complexity and
 489 modeling error. Unlike classical algorithms, it will thus learn LSSMs with only the minimally
 490 required parameters to explain the time-series data. In particular, if the real-world systems are
 491 identifiable, the proposed algorithm preserves the topological structure among variables, which is
 492 more valuable for exploring interaction laws of systems.

494 6 DISCUSSION

497 To learn the LSSMs with sparse system matrices, we impose sparsity-promoting priors on system
 498 matrices to balance model complexity and modeling error. Following the MAP principle, we then
 499 learn system matrices by exploring the EM algorithm to maximize the joint posterior distribution
 500 composed of the priors and marginal likelihood function. Based on the Global Convergence The-
 501 orem, we demonstrate that the sequence generated by the proposed algorithm converges to a local
 502 maximum or saddle point of the posterior distribution. In addition, we explain why the sparsity-
 503 promoting prior is capable of retaining the inherent topological structure of LSSMs, as the non-
 504 singular matrix of the similarity transformation is limited to be a generalized permutation matrix.
 505 Hence, the proposed algorithm is more useful for us to explore the interaction laws of LSSMs com-
 506 pared to the classical ones.

507 There still remain some potential limitations associated with the proposed algorithm. First, the
 508 similarity transformation may shrink many parameters in system matrices to very small values,
 509 potentially leading to numerical errors. However, note that it is a common issue faced by all the
 510 learning algorithms for LSSMs. The other limitation is that the proposed algorithm is hard to deal
 511 with large-scale problems currently due to its high computational requirements. [Hence, our future](#)
 512 [work will focus on reducing computation time to make the proposed algorithm applicable to large-](#)
 513 [scale settings. For instance, we can adopt the stochastic EM algorithm to reduce the computational](#)
 514 [cost by using a mini-batch of data instead of the full batch during the expectation step](#) (Chen et al.,
 515 2018). In addition, we hope to explore how to ensure that the learned system matrices are exactly
 516 the same as the true ones by imposing additional constraints on system matrices beyond the sparsity
 517 constraint. Overall, we believe that the proposed algorithm sheds light on the learning of LSSMs
 518 with sparse system matrices.

519 ETHICS STATEMENT

520 This paper presents theoretical research whose goal is to advance the field of Machine Learning.
 521 Because it does not involve human participants, animals, sensitive personal data, or other foreseeable
 522 ethical concerns outlined in the ICLR Code of Ethics, no specific ethical issues arise from this paper.

525 REPRODUCIBILITY STATEMENT

526 To ensure the reproducibility of this research, the main text and Appendix provide detailed theoreti-
 527 cal derivations and proofs of the proposed algorithm, and the complete source code is included in the
 528 supplementary material to enable independent verification. Moreover, the real-world datasets used
 529 in our experiments are publicly available at [https://homes.esat.kuleuven.be/~smc/](https://homes.esat.kuleuven.be/~smc/daisy/)
 530 [daisy/](#).

533 REFERENCES

534
 535 Ainesh Bakshi, Allen Liu, Ankur Moitra, and Morris Yau. Tensor decompositions meet control
 536 theory: learning general mixtures of linear dynamical systems. In *International Conference on*
 537 *Machine Learning*, pp. 1549–1563. PMLR, 2023.

538
 539 David Belanger and Sham Kakade. A linear dynamical system model for text. In *International*
 540 *Conference on Machine Learning*, pp. 833–842. PMLR, 2015.

540 Steven L Brunton, Joshua L Proctor, and J Nathan Kutz. Discovering governing equations from data
 541 by sparse identification of nonlinear dynamical systems. *Proceedings of the National Academy of*
 542 *Sciences*, 113(15):3932–3937, 2016.

543

544 Emmanuel J Candes, Michael B Wakin, and Stephen P Boyd. Enhancing sparsity by reweighted ℓ_1
 545 minimization. *Journal of Fourier Analysis and Applications*, 14:877–905, 2008.

546

547 Nilanjana Chakraborty, Kshitij Khare, and George Michailidis. A Bayesian framework for sparse
 548 estimation in high-dimensional mixed frequency vector autoregressive models. *Statistica Sinica*,
 549 33:1629–1652, 2023.

550

551 Jianfei Chen, Jun Zhu, Yee Whye Teh, and Tong Zhang. Stochastic expectation maximization with
 552 variance reduction. In *Advances in Neural Information Processing Systems*, volume 31, 2018.

553

554 Yanxi Chen and H Vincent Poor. Learning mixtures of linear dynamical systems. In *International*
 555 *Conference on Machine Learning*, pp. 3507–3557. PMLR, 2022.

556

557 Kevin Course and Prasanth B Nair. State estimation of a physical system with unknown governing
 558 equations. *Nature*, 622(7982):261–267, 2023.

559

560 Yonathan Efroni, Sham Kakade, Akshay Krishnamurthy, and Cyril Zhang. Sparsity in partially
 561 controllable linear systems. In *International Conference on Machine Learning*, pp. 5851–5860.
 562 PMLR, 2022.

563

564 Mohamad Kazem Shirani Faradonbeh, Ambuj Tewari, and George Michailidis. Finite time identifi-
 565 cation in unstable linear systems. *Automatica*, 96:342–353, 2018.

566

567 Mohamad Kazem Shirani Faradonbeh, Ambuj Tewari, and George Michailidis. Optimism-based
 568 adaptive regulation of linear-quadratic systems. *IEEE Transactions on Automatic Control*, 66(4):
 569 1802–1808, 2020.

570

571 Wouter Favoreel, Bart De Moor, and Peter Van Overschee. Subspace state space system identifica-
 572 tion for industrial processes. *Journal of Process Control*, 10(2-3):149–155, 2000.

573

574 Zoubin Ghahramani and Geoffrey E Hinton. Parameter estimation for linear dynamical systems.
 575 1996.

576

577 Stuart Gibson and Brett Ninness. Robust maximum-likelihood estimation of multivariable dynamic
 578 systems. *Automatica*, 41(10):1667–1682, 2005.

579

580 Elad Hazan, Singh Karan, and Zhang Cyril. Learning linear dynamical systems via spectral filtering.
 581 In *Advances in Neural Information Processing Systems*, volume 30, 2017.

582

583 Jiabao He, Ingvar Ziemann, Cristian R Rojas, and Håkan Hjalmarsson. Finite sample analysis for
 584 a class of subspace identification methods. In *IEEE Conference on Decision and Control*, pp.
 585 2970–2976. IEEE, 2024a.

586

587 Xin He, Yasen Wang, and Junyang Jin. Bayesian inference and optimisation of stochastic dynamical
 588 networks. *International Journal of Systems Science*, pp. 1–15, 2024b.

589

590 Wenbing Huang, Lele Cao, Fuchun Sun, Deli Zhao, Huaping Liu, and Shanshan Yu. Learning
 591 stable linear dynamical systems with the weighted least square method. In *International Joint*
 592 *Conferences on Artificial Intelligence*, pp. 1599–1605, 2016.

593

594 Junyang Jin, Ye Yuan, and Jorge Gonçalves. A full Bayesian approach to sparse network inference
 595 using heterogeneous datasets. *IEEE Transactions on Automatic Control*, 66(7):3282–3288, 2020a.

596

597 Junyang Jin, Ye Yuan, and Jorge Gonçalves. High precision variational Bayesian inference of sparse
 598 linear networks. *Automatica*, 118:109017, 2020b.

599

600 Tohru Katayama et al. *Subspace methods for system identification*, volume 1. Springer, 2005.

601

602 Wallace E Larimore. Canonical variate analysis in identification, filtering, and adaptive control. In
 603 *IEEE Conference on Decision and Control*, pp. 596–604. IEEE, 1990.

594 Roderick JA Little and Donald B Rubin. *Statistical analysis with missing data*, volume 793. John
 595 Wiley & Sons, 2019.
 596

597 Lennart Ljung. Prediction error estimation methods. *Circuits, Systems and Signal Processing*, 21:
 598 11–21, 2002.

599 David G Luenberger, Yinyu Ye, et al. *Linear and nonlinear programming*, volume 2. Springer,
 600 1984.
 601

602 Bethany Lusch, J Nathan Kutz, and Steven L Brunton. Deep learning for universal linear embeddings
 603 of nonlinear dynamics. *Nature Communications*, 9(1):4950, 2018.

604 Giorgos Mamakoukas, Maria Castano, Xiaobo Tan, and Todd Murphrey. Local Koopman operators
 605 for data-driven control of robotic systems. In *Robotics: Science and Systems*, 2019.

606 Giorgos Mamakoukas, Orest Xherija, and Todd Murphrey. Memory-efficient learning of stable linear
 607 dynamical systems for prediction and control. In *Advances in Neural Information Processing
 608 Systems*, pp. 13527–13538, 2020.

609

610 James Martens. Learning the linear dynamical system with ASOS. In *International Conference on
 611 Machine Learning*, pp. 743–750. Citeseer, 2010.

612

613 Aditya Modi, Mohamad Kazem Shirani Faradonbeh, Ambuj Tewari, and George Michailidis. Joint
 614 learning of linear time-invariant dynamical systems. *Automatica*, 164:111635, 2024.

615

616 Samet Oymak and Necmiye Ozay. Non-asymptotic identification of lti systems from a single trajec-
 617 tory. In *American Control Conference*, pp. 5655–5661. IEEE, 2019.

618 Wei Pan, Ye Yuan, Jorge Gonçalves, and Guy-Bart Stan. A sparse Bayesian approach to the identifi-
 619 cation of nonlinear state-space systems. *IEEE Transactions on Automatic Control*, 61(1):182–187,
 620 2015.

621

622 G Pillonetto and Lennart Ljung. Full Bayesian identification of linear dynamic systems using stable
 623 kernels. *Proceedings of the National Academy of Sciences*, 120(18):e2218197120, 2023.

624

625 S Joe Qin. An overview of subspace identification. *Computers & Chemical Engineering*, 30:1502–
 1513, 2006.

626

627 Srijata Samanta, Kshitij Khare, and George Michailidis. A generalized likelihood-based Bayesian
 628 approach for scalable joint regression and covariance selection in high dimensions. *Statistics and
 629 Computing*, 32(3):47, 2022.

630

631 Simo Särkkä and Lennart Svensson. *Bayesian filtering and smoothing*, volume 17. Cambridge
 632 University Press, 2023.

633

634 Robert H Shumway and David S Stoffer. An approach to time series smoothing and forecasting
 using the EM algorithm. *Journal of Time Series Analysis*, 3(4):253–264, 1982.

635

636 Gavin Smith, João de Freitas, Tony Robinson, and Mahesan Niranjan. Speech modelling using
 637 subspace and EM techniques. In *Advances in Neural Information Processing Systems*, volume 12,
 1999.

638

639 Robert Tibshirani. Regression shrinkage and selection via the Lasso. *Journal of the Royal Statistical
 640 Society Series B: Statistical Methodology*, 58(1):267–288, 1996.

641

642 Michael E Tipping. Sparse Bayesian learning and the relevance vector machine. *Journal of Machine
 643 Learning Research*, 1:211–244, 2001.

644

645 Jack Umenberger, Johan Wågberg, Ian R Manchester, and Thomas B Schön. Maximum likelihood
 646 identification of stable linear dynamical systems. *Automatica*, 96:280–292, 2018.

647

Peter Van Overschee and Bart De Moor. N4SID: Subspace algorithms for the identification of
 combined deterministic-stochastic systems. *Automatica*, 30(1):75–93, 1994.

648 Peter Van Overschee and BL De Moor. *Subspace identification for linear systems: Theory—Implementation—Applications*. Springer Science & Business Media, 2012.
 649
 650

651 M Verahegen and Patrick Dewilde. Subspace model identification. Part i: The output-error state-
 652 space model identification class of algorithm. *International Journal of Control*, 56:1187–1210,
 653 1992.

654 Mats Viberg. Subspace methods in system identification. *IFAC Proceedings Volumes*, 27(8):1–12,
 655 1994.
 656

657 Jin Wang and S Joe Qin. A new subspace identification approach based on principal component
 658 analysis. *Journal of Process Control*, 12(8):841–855, 2002.

659 Yasen Wang, Junlin Li, Zuogong Yue, and Ye Yuan. An iterative Min-Min optimization method for
 660 sparse Bayesian learning. In *International Conference on Machine Learning*, volume 235, pp.
 661 50859–50873, 2024.

662 David Wipf and Srikantan Nagarajan. A new view of automatic relevance determination. In *Ad-
 663 vances in Neural Information Processing Systems*, volume 20, 2007.

664 David P Wipf and Bhaskar D Rao. Sparse Bayesian learning for basis selection. *IEEE Transactions
 665 on Signal Processing*, 52(8):2153–2164, 2004.

666 CF Jeff Wu. On the convergence properties of the EM algorithm. *The Annals of Statistics*, pp.
 667 95–103, 1983.

668 Xiaofeng Yuan, Yalin Wang, Chunhua Yang, Zhiqiang Ge, Zhihuan Song, and Weihua Gui.
 669 Weighted linear dynamic system for feature representation and soft sensor application in nonlin-
 670 ear dynamic industrial processes. *IEEE Transactions on Industrial Electronics*, 65(2):1508–1517,
 671 2017.

672 Ye Yuan, Xiuchuan Tang, Wei Zhou, Wei Pan, Xiuting Li, Hai-Tao Zhang, Han Ding, and Jorge
 673 Goncalves. Data driven discovery of cyber physical systems. *Nature Communications*, 10(1):
 674 4894, 2019.

675 Wei Zhou, Hai-Tao Zhang, and Jun Wang. An efficient sparse Bayesian learning algorithm based on
 676 Gaussian-scale mixtures. *IEEE Transactions on Neural Networks and Learning Systems*, 33(7):
 677 3065–3078, 2021.

678 Yucai Zhu, Peter Van Overschee, Ban de Moor, and Lennan Ljung. Comparison of three classes of
 679 identification methods. *IFAC Proceedings Volumes*, 27(8):169–174, 1994.
 680
 681
 682
 683
 684
 685
 686
 687
 688
 689
 690
 691
 692
 693
 694
 695
 696
 697
 698
 699
 700
 701

702 **A SPARSITY-PROMOTING PRIOR**
 703

704 Besides \mathbf{A} , we also impose the sparsity-promoting priors on \mathbf{B} , \mathbf{C} , and \mathbf{D} as follows:
 705

$$706 \quad p(\mathbf{B} | \boldsymbol{\Gamma}_b) = \prod_{i=1}^n \prod_{j=1}^p p(\mathbf{B}_{ij} | \boldsymbol{\Gamma}_{b,ij}) = \prod_{i=1}^n \prod_{j=1}^p \frac{1}{\sqrt{2\pi\boldsymbol{\Gamma}_{b,ij}}} \exp\left(-\frac{\mathbf{B}_{ij}^2}{2\boldsymbol{\Gamma}_{b,ij}}\right), \quad (38)$$

$$709 \quad p(\mathbf{C} | \boldsymbol{\Gamma}_c) = \prod_{i=1}^m \prod_{j=1}^n p(\mathbf{C}_{ij} | \boldsymbol{\Gamma}_{c,ij}) = \prod_{i=1}^m \prod_{j=1}^n \frac{1}{\sqrt{2\pi\boldsymbol{\Gamma}_{c,ij}}} \exp\left(-\frac{\mathbf{C}_{ij}^2}{2\boldsymbol{\Gamma}_{c,ij}}\right), \quad (39)$$

$$712 \quad p(\mathbf{D} | \boldsymbol{\Gamma}_d) = \prod_{i=1}^m \prod_{j=1}^p p(\mathbf{D}_{ij} | \boldsymbol{\Gamma}_{d,ij}) = \prod_{i=1}^m \prod_{j=1}^p \frac{1}{\sqrt{2\pi\boldsymbol{\Gamma}_{d,ij}}} \exp\left(-\frac{\mathbf{D}_{ij}^2}{2\boldsymbol{\Gamma}_{d,ij}}\right), \quad (40)$$

715 where $\boldsymbol{\Gamma}_{b,ij}$, $\boldsymbol{\Gamma}_{c,ij}$, and $\boldsymbol{\Gamma}_{d,ij}$ are the ij th components of $\boldsymbol{\Gamma}_b$, $\boldsymbol{\Gamma}_c$, and $\boldsymbol{\Gamma}_d$, respectively. To complete
 716 the hierarchy, the Inverse-Gamma distribution prior is imposed on each component of $\boldsymbol{\Gamma}_b$, $\boldsymbol{\Gamma}_c$, and
 717 $\boldsymbol{\Gamma}_d$ as follows:
 718

$$719 \quad p(\boldsymbol{\Gamma}_b) = \prod_{i=1}^n \prod_{j=1}^p \frac{a_0^{b_0}}{\Gamma(a_0)} \boldsymbol{\Gamma}_{b,ij}^{-a_0-1} \exp\left(-\frac{b_0}{\boldsymbol{\Gamma}_{b,ij}}\right), \quad (41)$$

$$722 \quad p(\boldsymbol{\Gamma}_c) = \prod_{i=1}^m \prod_{j=1}^n \frac{a_0^{b_0}}{\Gamma(a_0)} \boldsymbol{\Gamma}_{c,ij}^{-a_0-1} \exp\left(-\frac{b_0}{\boldsymbol{\Gamma}_{c,ij}}\right), \quad (42)$$

$$725 \quad p(\boldsymbol{\Gamma}_d) = \prod_{i=1}^m \prod_{j=1}^p \frac{a_0^{b_0}}{\Gamma(a_0)} \boldsymbol{\Gamma}_{d,ij}^{-a_0-1} \exp\left(-\frac{b_0}{\boldsymbol{\Gamma}_{d,ij}}\right). \quad (43)$$

727
 728
 729
 730
 731
 732
 733
 734
 735
 736
 737
 738
 739
 740
 741
 742
 743
 744
 745
 746
 747
 748
 749
 750
 751
 752
 753
 754
 755

756 **B DETAILED MATHEMATICAL DERIVATION**
 757

758 **B.1 DERIVATION OF EQUATION 15**
 759

760 Given the conditional independence between the variables, we can derive
 761

$$\begin{aligned}
 & H(\Theta | \Theta^k) \\
 &= \mathbb{E}_{\mathbf{X}^k} [\log(p(\mathbf{Y}, \mathbf{X} | \Theta)p(\Theta))] \\
 &= \mathbb{E}_{\mathbf{X}^k} [\log(p(\mathbf{Y} | \mathbf{X}, \Theta)p(\mathbf{X} | \Theta)p(\Theta))] \\
 &= \mathbb{E}_{\mathbf{X}^k} [\log(p(\mathbf{Y} | \mathbf{X}, \mathbf{C}, \mathbf{D}, \mathbf{Q})p(\mathbf{X} | \mathbf{A}, \mathbf{B}, \mathbf{R})p(\mathbf{A}, \Gamma_a, \mathbf{B}, \Gamma_b, \mathbf{C}, \Gamma_c, \mathbf{D}, \Gamma_d))] \\
 &= \mathbb{E}_{\mathbf{X}^k} [\log(p(\mathbf{Y} | \mathbf{X}, \mathbf{C}, \mathbf{D}, \mathbf{Q})p(\mathbf{X} | \mathbf{A}, \mathbf{B}, \mathbf{R})p(\mathbf{A}, \Gamma_a)p(\mathbf{B}, \Gamma_b)p(\mathbf{C}, \Gamma_c)p(\mathbf{D}, \Gamma_d))] \\
 &= \underbrace{\mathbb{E}_{\mathbf{X}^k} [\log p(\mathbf{X} | \mathbf{A}, \mathbf{B}, \mathbf{R})]}_{H_1(\mathbf{A}, \mathbf{B}, \mathbf{R})} + \underbrace{\mathbb{E}_{\mathbf{X}^k} [\log p(\mathbf{Y} | \mathbf{X}, \mathbf{C}, \mathbf{D}, \mathbf{Q})]}_{H_2(\mathbf{C}, \mathbf{D}, \mathbf{Q})} \\
 &\quad + \underbrace{\mathbb{E}_{\mathbf{X}^k} [\log(p(\mathbf{A}, \Gamma_a)p(\mathbf{B}, \Gamma_b)p(\mathbf{C}, \Gamma_c)p(\mathbf{D}, \Gamma_d))]}_{H_3(\mathbf{A}, \mathbf{B}, \mathbf{C}, \mathbf{D}, \Gamma_a, \Gamma_b, \Gamma_c, \Gamma_d)}. \tag{44}
 \end{aligned}$$

774
 775 **Explicit mathematical expression of $H_1(\mathbf{A}, \mathbf{B}, \mathbf{R})$.** Based on equation 1 and the chain rule in
 776 probability, we can derive

$$\begin{aligned}
 & p(\mathbf{X} | \mathbf{A}, \mathbf{B}, \mathbf{R}) \\
 &= p(\mathbf{x}_0) \prod_{t=1}^T p(\mathbf{x}_t | \mathbf{x}_{t-1}, \mathbf{A}, \mathbf{B}, \mathbf{R}) \\
 &\propto \prod_{t=1}^T |\mathbf{R}|^{-\frac{1}{2}} \exp \left(-\frac{(\mathbf{x}_t - \mathbf{A}\mathbf{x}_{t-1} - \mathbf{B}\mathbf{u}_t)' \mathbf{R}^{-1} (\mathbf{x}_t - \mathbf{A}\mathbf{x}_{t-1} - \mathbf{B}\mathbf{u}_t)}{2} \right). \tag{45}
 \end{aligned}$$

785 Hence,

$$\begin{aligned}
 & H_1(\mathbf{A}, \mathbf{B}, \mathbf{R}) \\
 &= \mathbb{E}_{\mathbf{X}^k} [\log p(\mathbf{X} | \mathbf{A}, \mathbf{B}, \mathbf{R})] \\
 &= \mathbb{E}_{\mathbf{X}^k} \left[-\frac{T \log |\mathbf{R}| + \sum_{t=1}^T (\mathbf{x}_t - \mathbf{A}\mathbf{x}_{t-1} - \mathbf{B}\mathbf{u}_t)' \mathbf{R}^{-1} (\mathbf{x}_t - \mathbf{A}\mathbf{x}_{t-1} - \mathbf{B}\mathbf{u}_t)}{2} \right] \\
 &= -\frac{T \log |\mathbf{R}| + \sum_{t=1}^T \mathbb{E}_{\mathbf{X}^k} [(\mathbf{x}_t - \mathbf{A}\mathbf{x}_{t-1} - \mathbf{B}\mathbf{u}_t)' \mathbf{R}^{-1} (\mathbf{x}_t - \mathbf{A}\mathbf{x}_{t-1} - \mathbf{B}\mathbf{u}_t)]}{2} \\
 &= -\frac{T \log |\mathbf{R}| + \sum_{t=1}^T (\mathbf{m}_t^k - \mathbf{A}\mathbf{m}_{t-1}^k - \mathbf{B}\mathbf{u}_t)' \mathbf{R}^{-1} (\mathbf{m}_t^k - \mathbf{A}\mathbf{m}_{t-1}^k - \mathbf{B}\mathbf{u}_t)}{2} \\
 &\quad - \frac{\sum_{t=1}^T (\text{Tr}(\mathbf{R}^{-1} \mathbf{P}_t^k) - \text{Tr}(\mathbf{R}^{-1} \mathbf{A} \mathbf{P}_{t,t-1}^k) - \text{Tr}(\mathbf{A}' \mathbf{R}^{-1} \mathbf{P}_{t,t-1}^k) + \text{Tr}(\mathbf{A}' \mathbf{R}^{-1} \mathbf{A} \mathbf{P}_{t-1}^k))}{2}. \tag{46}
 \end{aligned}$$

801
 802 **Explicit mathematical expression of $H_2(\mathbf{C}, \mathbf{D}, \mathbf{Q})$.** Based on equation 2, we can derive

$$\begin{aligned}
 & p(\mathbf{Y} | \mathbf{X}, \mathbf{C}, \mathbf{D}, \mathbf{Q}) \\
 &= \prod_{t=1}^T p(\mathbf{y}_t | \mathbf{x}_t, \mathbf{C}, \mathbf{D}) \\
 &\propto \prod_{t=1}^T |\mathbf{Q}|^{-\frac{1}{2}} \exp \left(-\frac{(\mathbf{y}_t - \mathbf{C}\mathbf{x}_t - \mathbf{D}\mathbf{u}_t)' \mathbf{Q}^{-1} (\mathbf{y}_t - \mathbf{C}\mathbf{x}_t - \mathbf{D}\mathbf{u}_t)}{2} \right). \tag{47}
 \end{aligned}$$

810 Hence,

$$\begin{aligned}
 812 \quad & H_2(\mathbf{C}, \mathbf{D}, \mathbf{Q}) \\
 813 \quad &= \mathbb{E}_{\mathbf{X}^k} [\log p(\mathbf{Y} \mid \mathbf{X}, \mathbf{C}, \mathbf{D}, \mathbf{Q})] \\
 814 \quad &= -\frac{\mathbb{E}_{\mathbf{X}^k} \left[T \log |\mathbf{Q}| + \sum_{t=1}^T (\mathbf{y}_t - \mathbf{C}\mathbf{x}_t - \mathbf{D}\mathbf{u}_t)' \mathbf{Q}^{-1} (\mathbf{y}_t - \mathbf{C}\mathbf{x}_t - \mathbf{D}\mathbf{u}_t) \right]}{2} \\
 815 \quad &= -\frac{T \log |\mathbf{Q}| + \sum_{t=1}^T \mathbb{E}_{\mathbf{X}^k} [(\mathbf{y}_t - \mathbf{C}\mathbf{x}_t - \mathbf{D}\mathbf{u}_t)' \mathbf{Q}^{-1} (\mathbf{y}_t - \mathbf{C}\mathbf{x}_t - \mathbf{D}\mathbf{u}_t)]}{2} \\
 816 \quad &= -\frac{T \log |\mathbf{Q}| + \sum_{t=1}^T ((\mathbf{y}_t - \mathbf{C}\mathbf{m}_t^k - \mathbf{D}\mathbf{u}_t)' \mathbf{Q}^{-1} (\mathbf{y}_t - \mathbf{C}\mathbf{m}_t^k - \mathbf{D}\mathbf{u}_t) + \text{Tr}(\mathbf{C}' \mathbf{Q}^{-1} \mathbf{C} \mathbf{P}_t^k))}{2}. \tag{48}
 \end{aligned}$$

823
 824 **Explicit mathematical expression of $H_3(\mathbf{A}, \mathbf{B}, \mathbf{C}, \mathbf{D}, \mathbf{\Gamma}_a, \mathbf{\Gamma}_b, \mathbf{\Gamma}_c, \mathbf{\Gamma}_d)$.** Based on the priors imposed on the system matrices and corresponding hyperparameters, we can derive:

$$\begin{aligned}
 826 \quad & p(\mathbf{A}, \mathbf{\Gamma}_a) p(\mathbf{B}, \mathbf{\Gamma}_b) p(\mathbf{C}, \mathbf{\Gamma}_c) p(\mathbf{D}, \mathbf{\Gamma}_d) \\
 827 \quad &= p(\mathbf{A} \mid \mathbf{\Gamma}_a) p(\mathbf{\Gamma}_a) p(\mathbf{B} \mid \mathbf{\Gamma}_b) p(\mathbf{\Gamma}_b) p(\mathbf{C} \mid \mathbf{\Gamma}_c) p(\mathbf{\Gamma}_c) p(\mathbf{D} \mid \mathbf{\Gamma}_d) p(\mathbf{\Gamma}_d) \\
 828 \quad &\propto \prod_{i=1}^n \prod_{j=1}^n \Gamma_{a,ij}^{-\frac{2a_0+3}{2}} \exp\left(-\frac{\mathbf{A}_{ij}^2 + 2b_0}{2\Gamma_{a,ij}}\right) \times \prod_{i=1}^n \prod_{j=1}^p \Gamma_{b,ij}^{-\frac{2a_0+3}{2}} \exp\left(-\frac{\mathbf{B}_{ij}^2 + 2b_0}{2\Gamma_{b,ij}}\right) \\
 829 \quad &\times \prod_{i=1}^m \prod_{j=1}^n \Gamma_{c,ij}^{-\frac{2a_0+3}{2}} \exp\left(-\frac{\mathbf{C}_{ij}^2 + 2b_0}{2\Gamma_{c,ij}}\right) \times \prod_{i=1}^m \prod_{j=1}^p \Gamma_{d,ij}^{-\frac{2a_0+3}{2}} \exp\left(-\frac{\mathbf{D}_{ij}^2 + 2b_0}{2\Gamma_{d,ij}}\right). \tag{49}
 \end{aligned}$$

835 Hence, we have

$$\begin{aligned}
 837 \quad & H_3(\mathbf{A}, \mathbf{B}, \mathbf{C}, \mathbf{D}, \mathbf{\Gamma}_a, \mathbf{\Gamma}_b, \mathbf{\Gamma}_c, \mathbf{\Gamma}_d) \\
 838 \quad &= \mathbb{E}_{\mathbf{X}^k} [\log (p(\mathbf{A}, \mathbf{\Gamma}_a) p(\mathbf{B}, \mathbf{\Gamma}_b) p(\mathbf{C}, \mathbf{\Gamma}_c) p(\mathbf{D}, \mathbf{\Gamma}_d))] \\
 839 \quad &= \mathbb{E}_{\mathbf{X}^k} [\log (p(\mathbf{A} \mid \mathbf{\Gamma}_a) p(\mathbf{\Gamma}_a) p(\mathbf{B} \mid \mathbf{\Gamma}_b) p(\mathbf{\Gamma}_b) p(\mathbf{C} \mid \mathbf{\Gamma}_c) p(\mathbf{\Gamma}_c) p(\mathbf{D} \mid \mathbf{\Gamma}_d) p(\mathbf{\Gamma}_d))] \\
 840 \quad &= -\sum_{i=1}^n \sum_{j=1}^n \left(\frac{(2a_0+3) \log |\mathbf{\Gamma}_{a,ij}|}{2} + \frac{\mathbf{A}_{ij}^2 + 2b_0}{2\Gamma_{a,ij}} \right) \\
 841 \quad &\quad - \sum_{i=1}^n \sum_{j=1}^p \left(\frac{(2a_0+3) \log |\mathbf{\Gamma}_{b,ij}|}{2} + \frac{\mathbf{B}_{ij}^2 + 2b_0}{2\Gamma_{b,ij}} \right) \\
 842 \quad &\quad - \sum_{i=1}^m \sum_{j=1}^n \left(\frac{(2a_0+3) \log |\mathbf{\Gamma}_{c,ij}|}{2} + \frac{\mathbf{C}_{ij}^2 + 2b_0}{2\Gamma_{c,ij}} \right) \\
 843 \quad &\quad - \sum_{i=1}^m \sum_{j=1}^p \left(\frac{(2a_0+3) \log |\mathbf{\Gamma}_{d,ij}|}{2} + \frac{\mathbf{D}_{ij}^2 + 2b_0}{2\Gamma_{d,ij}} \right). \tag{50}
 \end{aligned}$$

B.2 DERIVATION OF EQUATION 19

855 Because $H_1(\mathbf{A}, \mathbf{B}, \mathbf{R})$ and $H_3(\mathbf{A}, \mathbf{B}, \mathbf{C}, \mathbf{D}, \mathbf{\Gamma}_a, \mathbf{\Gamma}_b, \mathbf{\Gamma}_c, \mathbf{\Gamma}_d)$ involve \mathbf{A} , we can derive the term
 856 related to \mathbf{A}_r at the k th iteration as follows:
 857

$$\begin{aligned}
 858 \quad & H_1(\mathbf{A}, \mathbf{B}^k, \mathbf{R}^k) + H_3(\mathbf{A}, \mathbf{B}^k, \mathbf{C}^k, \mathbf{D}^k, \mathbf{\Gamma}_a^k, \mathbf{\Gamma}_b^k, \mathbf{\Gamma}_c^k, \mathbf{\Gamma}_d^k) \\
 859 \quad &= -\frac{\sum_{t=1}^T \sum_{r=1}^n (\mathbf{R}_{rr}^k)^{-1} \left(\text{Tr}(\mathbf{A}_r' \mathbf{A}_r \mathbf{P}_{t-1}^k) - 2\mathbf{A}_r (\mathbf{P}_{t,t-1,r}^k)' \right) + \sum_{r=1}^n \mathbf{A}_r \mathbf{\Gamma}_{a,r}^{kd} \mathbf{A}_r'}{2} \\
 860 \quad &\quad - \frac{\sum_{t=1}^T \sum_{r=1}^n (\mathbf{R}_{rr}^k)^{-1} (\mathbf{m}_{t,r}^k - \mathbf{A}_r \mathbf{m}_{t-1}^k - \mathbf{B}_r^k \mathbf{u}_t) (\mathbf{m}_{t,r}^k - \mathbf{A}_r \mathbf{m}_{t-1}^k - \mathbf{B}_r^k \mathbf{u}_t)'}{2} + c, \tag{51}
 \end{aligned}$$

where c is the term independent of \mathbf{A}_r . Hence, we can calculate the derivative of $H(\Theta \mid \Theta^k)$ with respect to \mathbf{A}_r as follows:

$$\begin{aligned}
& \frac{\partial H(\Theta | \Theta^k)}{\partial \mathbf{A}_r} \\
&= \frac{\partial H_1(\mathbf{A}, \mathbf{B}^k, \mathbf{R}^k)}{\partial \mathbf{A}_r} + \frac{\partial H_3(\mathbf{A}, \mathbf{B}^k, \mathbf{C}^k, \mathbf{D}^k, \mathbf{\Gamma}_a^k, \mathbf{\Gamma}_b^k, \mathbf{\Gamma}_c^k, \mathbf{\Gamma}_d^k)}{\partial \mathbf{A}_r} \\
&= \sum_{t=1}^T (\mathbf{R}_{rr}^k)^{-1} \left(\mathbf{P}_{t,t-1,r}^k + (\mathbf{m}_{t,r}^k - \mathbf{A}_r \mathbf{m}_{t-1}^k - \mathbf{B}_r^k \mathbf{u}_t) (\mathbf{m}_{t-1}^k)' - \mathbf{A}_r \mathbf{P}_{t-1}^k \right) - \mathbf{A}_r \bar{\mathbf{\Gamma}}_{a,r}^{kd}. \quad (52)
\end{aligned}$$

Setting equation 52 to zero leads to

$$\sum_{t=1}^T \mathbf{A}_r \left(\mathbf{m}_{t-1}^k \left(\mathbf{m}_{t-1}^k \right)' + \mathbf{P}_{t-1}^k \right) + \mathbf{A}_r \mathbf{R}_{rr}^k \bar{\boldsymbol{\Gamma}}_{a,r}^{kd} = \sum_{t=1}^T \left(\mathbf{P}_{t,t-1,r}^k + \left(\mathbf{m}_{t,r}^k - \mathbf{B}_r^k \mathbf{u}_t \right) \left(\mathbf{m}_{t-1}^k \right)' \right). \quad (53)$$

Hence, we can update A_r at the k th iteration as follows:

$$\begin{aligned} \mathbf{A}_r^{k+1} &= \left(\sum_{t=1}^T \left((\mathbf{m}_{t,r}^k - \mathbf{B}_r^k \mathbf{u}_t) (\mathbf{m}_{t-1}^k)' + \mathbf{P}_{t,t-1,r}^k \right) \right. \\ &\quad \times \left. \left(\sum_{t=1}^T \left(\mathbf{P}_{t-1}^k + \mathbf{m}_{t-1}^k (\mathbf{m}_{t-1}^k)' \right) + \mathbf{R}_{rr}^k \mathbf{\Gamma}_{a,r}^{kd} \right) \right)^{-1}. \end{aligned} \quad (54)$$

B.3 DERIVATION OF EQUATION 24

Given that R is a diagonal matrix, we can re-express $H_1(A^{k+1}, B^{k+1}, R)$ as follows:

$$H_1(\mathbf{A}^{k+1}, \mathbf{B}^{k+1}, \mathbf{R}) = -\frac{T \sum_{r=1}^n \log \mathbf{R}_{rr}}{2} - \frac{\sum_{r=1}^n \sum_{t=1}^T \mathbf{R}_{rr}^{-1} (\boldsymbol{\pi}_{t,r}^k)^2}{2} - \frac{\sum_{r=1}^n \sum_{t=1}^T \mathbf{R}_{rr}^{-1} \boldsymbol{\Pi}_{t,rr}^k}{2}, \quad (55)$$

where

$$\pi_t^k = m_t^k - A^{k+1}m_{t-1}^k - B^{k+1}u_t, \quad (56)$$

$$\Pi_t^k = P_t^k - A^{k+1} P_{t-1}^k - P_{t-1}^k (A^{k+1})' + A^{k+1} P_{t-1}^k (A^{k+1})' \quad (57)$$

with $\pi_{t,r}^k$ and $\Pi_{t,rr}^k$ being the r th and rr th components of π_t^k and Π_t^k , respectively. Hence, we can calculate the derivative of $H(\Theta | \Theta^k)$ with respect to R_{rr} as follows:

$$\frac{\partial H(\Theta | \Theta^k)}{\partial \mathbf{R}_{rr}} = \frac{\partial H_1(A^{k+1}, \mathbf{B}^{k+1}, \mathbf{R})}{\partial \mathbf{R}_{rr}} = -\frac{T}{2\mathbf{R}_{rr}} + \frac{\sum_{t=1}^T (\pi_{t,r}^k)^2}{2\mathbf{R}_{rr}^2} + \frac{\sum_{t=1}^T \Pi_{t,rr}^k}{2\mathbf{R}_{rr}^2}. \quad (58)$$

Setting equation 58 to zero leads to the update rule for \mathbf{R}_{xx} at the k th iteration as follows:

$$\mathbf{R}_{rr}^{k+1} = \frac{\sum_{t=1}^T (\boldsymbol{\pi}_{t,r}^k)^2 + \sum_{t=1}^T \mathbf{\Pi}_{t,rr}^k}{T}. \quad (59)$$

918 C PSEUDOCODE FOR LEARNING LSSMs WITH SPARSE SYSTEM MATRICES
919920 **Algorithm 1** The proposed algorithm for learning LSSMs with sparse system matrices
921

922 **Input:** Time-series data $\{(\mathbf{u}_t, \mathbf{y}_t)\}_{t=1}^T$, initial guess of Θ , and maximum number of iterations
923 k_{max}
924 **for** $k = 1$ **to** k_{max} **do**
925 **for** $t = 1$ **to** T **do**
926 Update the mean \mathbf{m}_t^k and covariance \mathbf{P}_t^k of \mathbf{x}_t via equation 9 and equation 10, respectively
927 Update the covariance $\mathbf{P}_{t,t-1}^k$ between \mathbf{x}_t and \mathbf{x}_{t-1} via equation 14
928 **end for**
929 Update system matrices \mathbf{A} , \mathbf{B} , \mathbf{C} , and \mathbf{D} via equation 20–equation 23, respectively
930 Update noise covariance matrices \mathbf{R} and \mathbf{Q} via equation 27 and equation 28, respectively
931 Update hyperparameter matrices Γ_a , Γ_b , Γ_c , and Γ_d via equation 31 and equation 32, respectively
932 **if** a stopping criterion is satisfied **then**
933 Break
934 **end if**
935 **end for**
936 **Output:** System matrices \mathbf{A} , \mathbf{B} , \mathbf{C} , and \mathbf{D} , noise covariance matrices \mathbf{R} and \mathbf{Q}

938 D PROOF OF THEOREM 3.3
939
940 *Proof.* To illustrate the global convergence of the proposed algorithm, we need to demonstrate that
941 it satisfies the three necessary conditions required by the Global Convergence Theorem (Luenberger
942 et al., 1984). **For $\mathcal{A}(\cdot)$ and $\Omega = \{\Theta : \nabla_{\Theta} p(\Theta | \mathbf{Y}) = \mathbf{0}\}$, $\mathcal{L}(\Theta) = -p(\Theta | \mathbf{Y})$ is a descent**
943 **function.** For the point Θ^k in Ω , it is straightforward to conclude that $\mathcal{L}(\Theta^{k+1}) \leq \mathcal{L}(\Theta^k)$
944 following the basic property of the EM algorithm. For the point Θ^k outside Ω , as $H(\Theta | \Theta^k)$ is
945 continuous in both arguments, we have $\mathcal{L}(\Theta^{k+1}) < \mathcal{L}(\Theta^k)$ (see Theorem 2 in Wu (1983)). Hence,
946 $\mathcal{L}(\Theta)$ is a descent function for Ω and $\mathcal{A}(\cdot)$. **The sequence $\{\Theta^k\}_{k=1}^{\infty}$ is contained in a compact set.**
947 If any component of Θ is unbounded, $\mathcal{L}(\Theta)$ tends to infinity. Given $\mathcal{L}(\Theta^{k+1}) \leq \mathcal{L}(\Theta^k)$, there
948 must exist a compact set containing the sequence $\{\Theta^k\}_{k=1}^{\infty}$. **The mapping $\mathcal{A}(\cdot)$ is closed at points**
949 **outside Ω .** Because the proposed algorithm updates Θ^{k+1} from Θ^k via analytical mathematical
950 expressions, and all elementary functions involved are continuous, $\mathcal{A}(\cdot)$ can thus be regarded as a
951 continuous function. In addition, $\mathcal{A}(\cdot)$ is a point-to-point mapping. Hence, $\mathcal{A}(\cdot)$ is closed at points
952 outside Ω (see Example 2 in Section 7.6 in Luenberger et al. (1984)). The proof is completed. \square
953
954
955
956
957
958
959
960
961
962
963
964
965
966
967
968
969
970
971

972 E EQUIVALENT REALIZATION OF LSSMs
973974 Based on the transformed coordinates, we can derive
975

976
$$\bar{x}_t = \Phi x_t = \Phi A x_{t-1} + \Phi B u_t + \Phi \varepsilon_t = (\Phi A \Phi^{-1}) \bar{x}_{t-1} + (\Phi B) u_t + \Phi \varepsilon_t, \quad (60)$$

977
$$y_t = C x_t + D u_t + \omega_t = (C \Phi^{-1}) \bar{x}_t + D u_t + \omega_t. \quad (61)$$

978 Hence, we can derive an equivalent realization of the original LSSM as follows:
979

980
$$\bar{x}_t = \bar{A} \bar{x}_{t-1} + \bar{B} u_t + \bar{\varepsilon}_t, \quad (62)$$

981
$$y_t = \bar{C} \bar{x}_t + \bar{D} u_t + \omega_t, \quad (63)$$

983 where $\bar{A} = \Phi A \Phi^{-1}$, $\bar{B} = \Phi B$, $\bar{C} = C \Phi^{-1}$, and $\bar{\varepsilon}_t = \Phi \varepsilon_t$. Because $\varepsilon_t \sim \mathcal{N}(\mathbf{0}, R)$, we can
984 derive the mean of $\bar{\varepsilon}_t$ as follows:
985

986
$$\mathbb{E}[\bar{\varepsilon}_t] = \mathbb{E}[\Phi \varepsilon_t] = \Phi \mathbb{E}[\varepsilon_t] = \mathbf{0}. \quad (64)$$

987 In addition, the covariance of $\bar{\varepsilon}_t$ can be derived as follows:
988

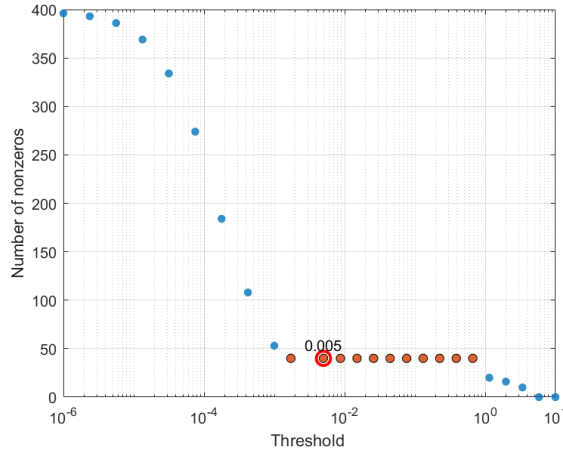
989
$$\mathbb{E}[(\bar{\varepsilon}_t - \mathbb{E}[\bar{\varepsilon}_t])(\bar{\varepsilon}_t - \mathbb{E}[\bar{\varepsilon}_t])'] = \mathbb{E}[\Phi \varepsilon_t \varepsilon_t' \Phi'] = \Phi \mathbb{E}[\varepsilon_t \varepsilon_t'] \Phi' = \Phi R \Phi'. \quad (65)$$

990 Hence, we have $\bar{\varepsilon}_t \sim \mathcal{N}(\mathbf{0}, \Phi R \Phi')$.
991992 F COMPUTATIONAL COMPLEXITY ANALYSIS
993994 The high computational cost of the proposed algorithm primarily stems from the matrix inversion
995 operations involved in closed-form updates. In each iteration, the expectation step entails the inver-
996 sion of matrices of size $n \times n$ and $m \times m$ a total of T times following Lemma 3.1. Hence, the
997 computational complexity of the expectation step is mainly determined by $\mathcal{O}(Tn^3 + Tm^3)$. In the
998 maximization step, we derive row-wise update rules for A , B , C , and D to enable analytical update
999 formulas. To update each row of A , B , C , and D , we need to calculate the inverses of the $n \times n$
1000 and $p \times p$ matrices as shown in equation 20–equation 23. As a result, the computational complexity
1001 of the maximization step is dominated by $\mathcal{O}((m+n)(n^3 + p^3))$. Because the computational cost
1002 of the proposed algorithm scales at least cubically with respect to one of m , n , and p , it is hard to
1003 deal with the large-scale problems currently. Hence, our future work will explore how to mitigate
1004 the computational bottleneck to make it more applicable.
1005
1006
1007
1008
1009
1010
1011
1012
1013
1014
1015
1016
1017
1018
1019
1020
1021
1022
1023
1024
1025

1026 **G THRESHOLD SELECTION**
1027

1028 While the proposed algorithm is globally convergent, the generated sequence converges to a local
 1029 maximum or saddle point of the posterior distribution only in the limit of infinite sequence length.
 1030 Hence, many learned parameters in system matrices approach zero but never reach it exactly during
 1031 algorithm implementation. To achieve accurate topology recovery, it is necessary to set the learned
 1032 parameters below a predefined threshold to zero to avoid numerical errors. In particular, the learned
 1033 parameters corresponding to the true zero components in the system matrices are typically several
 1034 orders of magnitude smaller than those learned for the nonzero components. Hence, this pronounced
 1035 difference in magnitude provides a wide and stable range for selecting the threshold.

1036 Specifically, the threshold can be selected by visualizing how the number of nonzero components in
 1037 learned system matrices, denoted as N , varies with the threshold. When the threshold is too small,
 1038 all components of learned system matrices remain nonzero, N is thus relatively large. As the thresh-
 1039 old increases, the learned parameters corresponding to the true zero components are gradually set
 1040 to zero, and N decreases accordingly. However, due to the pronounced difference in magnitude be-
 1041 tween the learned parameters corresponding to the true zero components and those corresponding to
 1042 the nonzero components, N remains stable over a certain range of threshold values. Once the thresh-
 1043 old exceeds this range, N begins to decrease again because some learned parameters corresponding
 1044 to true nonzero components are also set to zero. Therefore, the threshold can be safely selected
 1045 from this stable interval to ensure reliable topology recovery. For example, Figure 2 illustrates the
 1046 number of nonzero components in the learned system matrices under different threshold settings for
 1047 the synthetic system in Section 5.1. The orange markers indicate the threshold values at which the
 1048 proposed algorithm successfully learns the inherent topological structure among the variables, and
 1049 the MRE remains unchanged. As such, we set the threshold to 0.005 in the experiment.



1066 Figure 2: The number of nonzero components in the learned system matrices across various thresh-
 1067 old settings. When the threshold lies within the interval marked by the orange dots, the proposed
 1068 algorithm can successfully recover the inherent topological structure among the variables, and the
 1069 MRE remains unchanged.

1070
 1071
 1072
 1073
 1074
 1075
 1076
 1077
 1078
 1079

1080 **H ADDITIONAL EXPERIMENTAL RESULTS ON THE SYNTHETIC SYSTEM**
10811082 **H.1 EXPERIMENTAL RESULTS UNDER DIFFERENT INITIAL VALUES**
10831084 To assess the sensitivity of the proposed algorithm to initial values, we further evaluate its per-
1085 formance on the synthetic system described in Section 5.1 by initializing the A, B, C, D, R , and Q
1086 as aI_{10} , where a varies from 0.6 to 1.4 in increments of 0.2.1087 Table 2 records whether the proposed algorithm successfully learns the topological structure of the
1088 system matrices and MRE defined in the paper. As observed from the table, the experimental results
1089 are consistent with those in Section 5.1, indicating that the proposed algorithm is robust to initial
1090 values. Remarkably, even when the initial state transition matrix A is unstable (i.e., $a > 1$), the
1091 proposed algorithm is still able to accurately learn the topological structure of the true system.
10921093 Table 2: Experimental results of the proposed algorithm on the 10-dimensional synthetic system
1094 across different initial values
1095

<i>a</i>	0.6	0.8	1	1.2	1.4
Success?	✓	✓	✓	✓	✓
MRE	5.70%	5.70%	5.70%	5.70%	5.69%

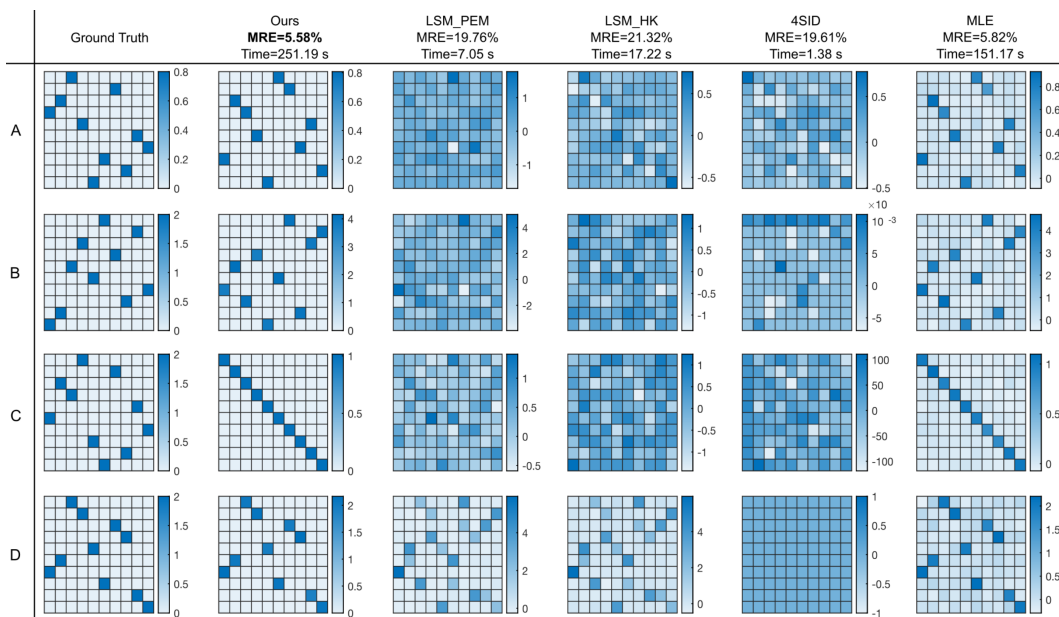
1100 **H.2 EXPERIMENTAL RESULTS OF INDEPENDENT TRIALS**
11011102 Here, we conduct 20 independent trials to demonstrate that the proposed algorithm is stable across
1103 multiple runs. Specifically, we set the random seed to increase evenly from 1 to 20. Table 3 reports
1104 the success rates of all the algorithms in learning the topological structure among the variables and
1105 the average MRE. Compared to the classical algorithms, only the proposed algorithm successfully
1106 learns the inherent topological structure among the variables in almost all cases. In addition, the
1107 proposed algorithm can achieve a 100% success rate by slightly increasing the threshold below
1108 which learned parameters are set to zero.
11091110 Table 3: Experimental results of all the algorithms on 20 independent trials
1111

Method	Ours	LSM PEM	LSM HK	4SID	MLE
Success rate	95%	0	0	0	0
Average MRE	5.67%	19.63%	21.56%	20.37%	5.97%

1134 **I EXPERIMENTAL RESULTS ON THE NON-DIAGONAL AND NON-INVERTIBLE**
 1135 **SYNTHETIC SYSTEMS**

1137 **I.1 NON-DIAGONAL SYSTEM**

1139 Here, we further test the proposed algorithm on a non-diagonal system to illustrate its effectiveness.
 1140 To generate non-diagonal system matrices, we randomly set one component per row to 0.8 in \mathbf{A} ,
 1141 and to 2 in \mathbf{B} , \mathbf{C} , and \mathbf{D} , with all other elements set to zero. Particularly, the nonzero elements
 1142 are deliberately placed to ensure that \mathbf{A} , \mathbf{B} , \mathbf{C} , and \mathbf{D} maintain full rank. All other experimental
 1143 settings remain the same as in Section 5.1.



1165 **Figure 3: Experimental results of all the algorithms on the non-diagonal systems.**

1166 Figure 3 records the experimental results of all the algorithms on the non-diagonal system. Due to
 1167 the similarity transformation as discussed in Section 4, the learned \mathbf{A} , \mathbf{B} , and \mathbf{C} of all the algorithms
 1168 differ in form from the ground truth. Unlike classical algorithms, however, the proposed algorithm
 1169 restricts the nonsingular matrix of the similarity transformation to be a generalized permutation
 1170 matrix. By comparing the learned \mathbf{B} and \mathbf{C} with ground truth, we can derive the nonsingular matrix
 1171 as follows:

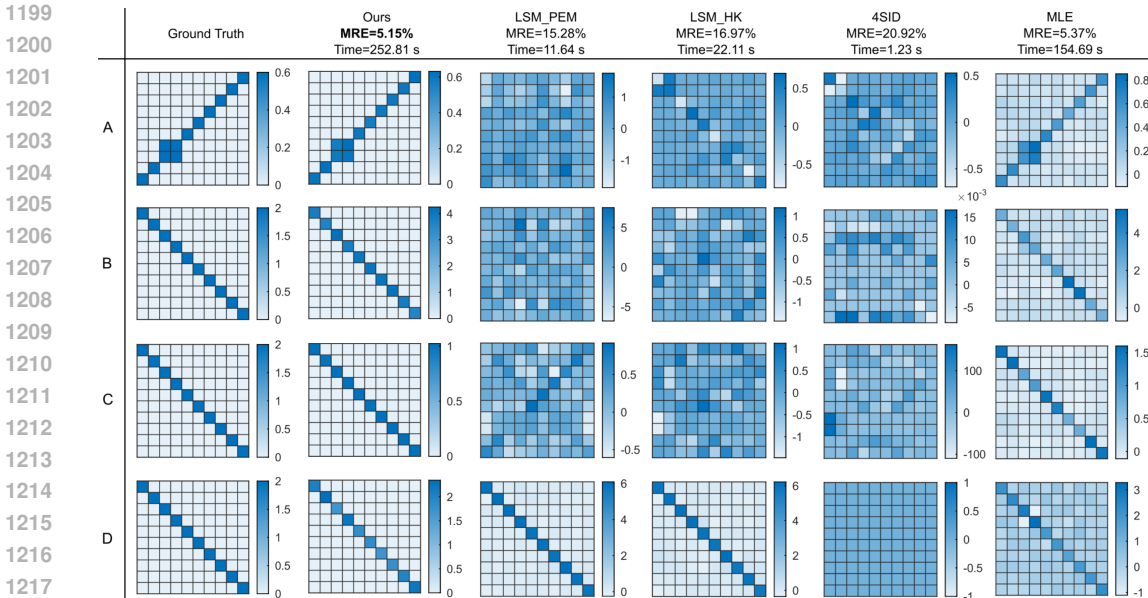
$$1174 \quad \Phi \approx \begin{bmatrix} 0 & 0 & 0 & 2 & 0 & 0 & 0 & 0 & 0 & 0 \\ 0 & 0 & 0 & 0 & 0 & 0 & 2 & 0 & 0 & 0 \\ 0 & 2 & 0 & 0 & 0 & 0 & 0 & 0 & 0 & 0 \\ 0 & 0 & 2 & 0 & 0 & 0 & 0 & 0 & 0 & 0 \\ 0 & 0 & 0 & 0 & 0 & 0 & 0 & 0 & 0 & 2 \\ 2 & 0 & 0 & 0 & 0 & 0 & 0 & 0 & 0 & 0 \\ 0 & 0 & 0 & 0 & 0 & 0 & 0 & 0 & 0 & 2 \\ 0 & 0 & 0 & 0 & 2 & 0 & 0 & 0 & 0 & 0 \\ 0 & 0 & 0 & 0 & 0 & 0 & 0 & 2 & 0 & 0 \\ 0 & 0 & 0 & 0 & 0 & 2 & 0 & 0 & 0 & 0 \end{bmatrix}. \quad (66)$$

1184 This implies that the discrepancy between the learned system matrices of the proposed algorithm
 1185 and ground truth stems from a different ordering and scaling of system states. Hence, it is easy
 1186 to check that the proposed algorithm still accurately captures the underlying system dynamics and
 1187 preserves the inherent topological structure among the variables.

1188
1189

I.2 NON-INVERTIBLE SYSTEM

1190 To evaluate the proposed algorithm on the non-invertible system, we replace the system matrix A
 1191 in the synthetic system of Section 5.1 with a singular matrix. Specifically, we first construct an anti-
 1192 diagonal matrix with all nonzero components set to 0.6, and then replace its seventh and eighth rows
 1193 with the following vector: [0 0 0.6 0.6 0 0 0 0 0 0]. As such, the seventh and eighth rows of A are
 1194 identical, making the matrix non-invertible. Besides, all other experimental settings remain the same
 1195 as in Section 5.1. Figure 4 reports the experimental results of all the algorithms on the non-invertible
 1196 system. Similarly, we can derive $\Phi \approx 2I_{10}$ by comparing the learned system matrices B and C
 1197 with the ground truth. Hence, the proposed algorithm still successfully preserves the topological
 1198 structure of system matrices, and obtains the lowest MRE compared to the other algorithms.
 1199

1220 Figure 4: Experimental results of all the algorithms on the non-invertible system.
 1221
 1222
 1223
 1224
 1225
 1226
 1227
 1228
 1229
 1230
 1231
 1232
 1233
 1234
 1235
 1236
 1237
 1238
 1239
 1240
 1241

1242 **J THE USE OF LARGE LANGUAGE MODELS (LLMS)**
1243

1244 In accordance with the ICLR policy on the use of large language models (LLMs), we declare that
1245 LLMs are only employed as a writing assistant to polish the language of this paper. They do not
1246 contribute to the research ideation, experimental design, data analysis, or interpretation of the results.
1247

1248
1249
1250
1251
1252
1253
1254
1255
1256
1257
1258
1259
1260
1261
1262
1263
1264
1265
1266
1267
1268
1269
1270
1271
1272
1273
1274
1275
1276
1277
1278
1279
1280
1281
1282
1283
1284
1285
1286
1287
1288
1289
1290
1291
1292
1293
1294
1295